

Follicular regulatory T cells restrain kidney allograft rejection in mice by suppressing alloreactive B cells

Received: 24 March 2024

Accepted: 24 February 2025

Published online: 04 March 2025



Hengcheng Zhang¹, Manuel A. Podestà^{1,7}, Cecilia B. Cavazzoni^{1,7}, Yumeng Wu¹, Jeong-Mi Lee¹, Xiaofei Li¹, Paulo Lisboa Raeder^{1,2}, Pragya Chandrakar¹, Maya Gempler¹, Sierra Richardson¹, Deepjyoti Ghosh³, Ismail Sayin⁴, Bruce R. Blazar⁵, Reza Abdi¹, Astrid Weins⁶, Anita S. Chong⁴ & Peter T. Sage¹✉

Pathogenic antibodies produced by alloreactive B cells mediate antibody-mediated rejection after kidney transplantation, but the mechanisms remain poorly understood. Follicular regulatory T (Tfr) cells modulate follicular helper T cell-mediated B cell responses, but the functions of Tfr in controlling alloreactive antibody are unknown. Here we study the developmental signals and functions of Tfr cells in mouse allogeneic kidney transplantation models, and show that costimulatory blockade alters the development of Tfr cells disproportionately by decreasing germinal center (GC)-like Tfr cells but increasing follicular-like Tfr cells. Functionally, global Tfr cell deletion results in accelerated graft rejection and increases in donor-specific B cells in both draining lymph nodes and kidney allografts. Mechanistically, Tfr cell deletion increases GC B cell expression of pro-inflammatory cytokines such as IL-15, while neutralization of IL-15 compensates for the loss of Tfr cells and prolongs the survival of mice receiving kidney transplants. Together our preclinical mouse data demonstrate how Tfr restrains kidney allograft rejection by limiting alloreactive B cell responses.

Solid organ transplantation is a crucial therapeutic intervention for patients with end-stage organ failure, not only improving survival but also substantially increasing recipient quality of life^{1,2}. Despite progress in the treatment of acute rejection with the development of broad immunosuppression, antibody-mediated rejection (ABMR) still represents the main cause of late graft failure with few, if any, successful treatments available^{3,4}. ABMR is also a barrier to clinical xenotransplantation, a potential source of donor organs^{5,6}. ABMR is facilitated by the formation of donor-specific antibodies (DSA), which

target allografts leading to endothelial injury and intimal arteritis, and ultimately graft loss⁷. Importantly, incidences of ABMR also include some degree of T cell mediated rejection (TCMR). Current therapeutic approaches for treating ABMR have focused on eliminating DSAs, but these methods have only minor clinical benefit and predispose recipients to opportunistic infections⁸. The development of new therapeutic strategies to treat ABMR is hindered by a limited understanding of the mechanisms controlling DSA formation and their roles in mediating ABMR. Part of this paucity of information is the lack

¹Transplantation Research Center, Renal Division, Brigham and Women's Hospital, Harvard Medical School, Boston, MA, USA. ²Department of Immunology, Institute of Biomedical Sciences, University of São Paulo, São Paulo, Brazil. ³Section of Rheumatology and The Knapp Center for Lupus and Immunology Research, Department of Medicine, The University of Chicago, Chicago, IL, USA. ⁴Department of Surgery, Section of Transplantation, University of Chicago, Chicago, IL, USA. ⁵Department of Pediatrics, Division of Blood & Marrow Transplant & Cellular Therapies, University of Minnesota, Minneapolis, MN, USA. ⁶Department of Pathology, Brigham and Women's Hospital, Harvard Medical School, Boston, MA, USA. ⁷These authors contributed equally: Manuel A. Podestà, Cecilia B. Cavazzoni. ✉e-mail: psage@bwh.harvard.edu

of studies in the context of allogeneic kidney transplantation, a setting in which ABMR is particularly relevant.

The majority of antibodies produced by B cells occur within lymphoid organs through a T cell-dependent process in which follicular helper T (T_{fh}) cells stimulate germinal center (GC) B cells to undergo clonal expansion, class switch recombination (CSR) and somatic hypermutation (SHM), thereby enhancing the pathogenic potential of antibodies^{9–11}. Follicular regulatory T (T_{fr}) cells provide a counterbalance to T_{fh} help by setting activation thresholds on GC B cells^{12–15}. T_{fr} cells are a specialized effector subset of regulatory T (T_{reg}) cell that expresses the transcription factor FoxP3 yet have transcriptional and phenotypic overlap with T_{fh} cells¹⁶. Newer data suggest that T_{fr} cells can exist in different phenotypic states, including a follicular phenotype marked by expression of CD25 as well as a GC-like phenotype in which CD25 is downregulated¹⁷. T_{fr} cells limit serological antibody responses specific for both autoreactive and foreign antigens, however their effect on autoreactive antibodies is more robust¹⁸. Recently, it was shown that T_{fr} cells can promote clonal diversity and affinity maturation of antibodies, suggesting that T_{fr} cells fine-tune activation thresholds on GC B cells instead of simply dampening antibody output¹⁹. Functionally, T_{fr} cells control developmental signals and cytokine production in T_{fh} cells, including IL-21 and IL-13^{18,20,21}. In the context of solid organ transplantation, T_{fh} cells have recently been shown to be key mediators of pathogenic B cell responses, DSA and ABMR^{22–25}. However, the roles of T_{fr} cells in the context of solid organ transplantation are less clear. Standard immunosuppression reduces T_{fr} cells, and the frequency of T_{fr} cells inversely correlates with ABMR in some clinical settings²⁶, however, an in-depth assessment of T_{fr} differentiation and function in controlling kidney transplant rejection has not been performed.

In this study, we investigate the developmental signals and functions of T_{fr} cells in the context of allogeneic kidney transplantation. Our results show that selective deletion of T_{fr} cells increased alloreactive B cell clones, DSA and ABMR-like disease. We also observe that T_{fr} cells limit the production of the pleiotropic cytokine IL-15 in GC B cells, and neutralization of IL-15 partially rescues the loss of T_{fr} cells. Together, these findings indicate that T_{fr} cells are critical in protecting kidney allografts from rejection. They suggest that targeted modulation of T_{fr} cells may offer a novel strategy to improve long-term transplant outcomes.

Results

Costimulatory blockade alters T_{fr} cell development after kidney transplantation

To study the development of T_{fr} cells during kidney transplantation, we used a previously described allogeneic kidney transplant model^{22,27}. We transplanted kidneys from allogeneic (Balb/c) or syngeneic (C57BL/6) mice into FoxP3 reporter (*Foxp3*^{IRE5-GFP}) mice on a C57BL/6 background. The spleen, draining lymph nodes (dLNs), graft, and blood were collected on days 10 and 20 post-transplantation (Fig. 1a). Allogeneic recipients exhibited a progressive ABMR-like disease, characterized by elevated serum IgG DSA levels and histological evidence of tubulitis and glomerulitis in the kidney grafts (Fig. 1b, c and Supplementary Fig. 1a). However, TCMR was also present. Although the frequency of total CD4⁺ T cells remained unchanged in dLN, there was a notable increase in T_{fh} (defined as CD4⁺CD19⁺CXCR5⁺FoxP3⁺) starting at day 10, as well as an increase in T_{fr} (CD4⁺CD19⁺CXCR5⁺FoxP3⁺) cells, but not until day 20 day after transplantation (Fig. 1d and Supplementary Fig. 1b). CD4⁺FoxP3⁺ cells in contrast did not change in frequency after allogeneic transplantation (Fig. 1e). Similarly to the dLN, splenic T_{fr} cell frequencies increased starting at day 20 after transplantation, whereas T_{fh} cells increased starting at day 10 (Supplementary Fig. 1c, d). Consistent with increases in T_{fh} and DSA, we found increases in the frequency of CD19⁺GL7⁺FAS⁺ germinal center (GC) B cells in both the dLN and spleen after allogeneic kidney transplantation compared to syngeneic controls

(Fig. 1f and Supplementary Fig. 1e). These findings indicate that T_{fr} cells differentiate after allogeneic kidney transplantation but with delayed kinetics compared to T_{fh} and GC B cells.

We next sought to determine the role of costimulation on T_{fr} cell development. CTLA4Ig, a T-cell costimulation blocker, is used in a subset of kidney transplant patients to prevent rejection, offering less toxicity than calcineurin inhibitors in some settings with similar graft survival rates^{28–30}. The impact of CTLA4Ig on T_{fr} development in the context of kidney transplantation remains unclear. To assess the role of systemic costimulatory blockade on T_{fr} differentiation, we administered CTLA4Ig two days after transplantation and assessed rejection (Fig. 1g). We observed similar levels of mononuclear cell infiltration with and without CTLA4Ig treatment (Fig. 1h). However, in the CTLA4Ig-treated group, mononuclear cells were predominantly localized to the renal interstitium and around arteries. In contrast, without treatment, the infiltrates were more diffusely distributed across glomeruli, tubules, and peritubular capillaries. Both groups showed high levels of TCMR-like pathological features, including interstitial inflammation and tubulitis (Supplementary Fig. 2a, b). CTLA4Ig treatment slightly reduced TCMR-like pathology but significantly decreased ABMR-associated pathological features, such as peritubular capillaritis and glomerulitis, and C4d deposition in grafts (Fig. 1h). CTLA4Ig treatment also reduced serological IgG DSA production starting on postoperative day 7 which continued until day 20 (Fig. 1i). CTLA4Ig treatment also resulted in a marked reduction in the frequencies of dLN GC B cells (Fig. 1j and Supplementary Fig. 2c). Although CTLA4Ig had a limited effect on the frequency of CD4⁺ T cell infiltration and effector T cell responses (Supplementary Fig. 2d–f), it had a significant inhibitory effect on total CXCR5⁺ follicular T cells as well as T_{fh} cells in dLN and peripheral blood, potentially by inducing apoptosis and anergy (Fig. 1k and Supplementary Fig. 3a–c). Furthermore, CTLA4Ig reduced the number of T_{fr} cells in the dLN and kidney allografts without altering the expression of the transcription factor FoxP3 (Supplementary Fig. 3d–f). ICOS expression was substantially lower on T_{fr} cells from CTLA4Ig-treated, compared to control, recipients (Supplementary Fig. 3g). Together these data demonstrate that while costimulatory blockade dampens T_{fh} and GC B cell differentiation, it also restrains T_{fr} cells.

Follicular to GC-like differentiation of T_{fr} cells is abrogated by costimulatory blockade

To characterize the developmental dynamics of T_{fr} cells and understand which specific stages are sensitive to costimulatory blockade, we performed single-cell RNA sequencing (scRNAseq) on sorted CD4⁺CD19⁺CXCR5⁺FoxP3⁺ T_{fr} and CD4⁺CD19⁺CXCR5⁺FoxP3⁺ T_{reg} cells from the dLN of allogeneic kidney transplant recipients, with or without CTLA4Ig treatment (Fig. 2a). Utilizing uniform manifold approximation and projection (UMAP) for dimensionality reduction, we identified 9 unique clusters from all cells (Fig. 2b and Supplementary Fig. 4a). T_{reg} cells predominantly occupied cluster 0 and portions of cluster 2. In contrast, T_{fr} cells occupied all other clusters as well as portions of cluster 2 (Fig. 2c and Supplementary Fig. 4b). All clusters expressed *Foxp3* and T_{fr}-containing clusters exhibited substantial expression of *Cxcr5* which is highly expressed in T_{fr} cells (Fig. 2d and Supplementary Fig. 4c). Next we assessed whether individual clusters of T_{fr} cells were reflective of distinct activation states. Cluster 0 and 6 which contained CXCR5⁺ Tregs but also some T_{fr} cells, had high expression of *Il2ra*/CD25 and the naïve T cell homing receptor *Sell*/CD62L (Fig. 2d, e and Supplementary Fig. 4c–e). We referred to these clusters as naïve-like clusters. Both *Sell* and *Il2ra* were also expressed in clusters 4 and 5, but these clusters also contained higher expression of the inducible costimulatory molecule *Icos* and to a lesser extent higher levels of *Cxcr5* compared to naïve-like cluster 0. Therefore, we referred to clusters 4 and 5 as “follicular-like” clusters. Interestingly, *Prdm1*/Blimp-1 was enriched in *Icos*-expressing clusters,

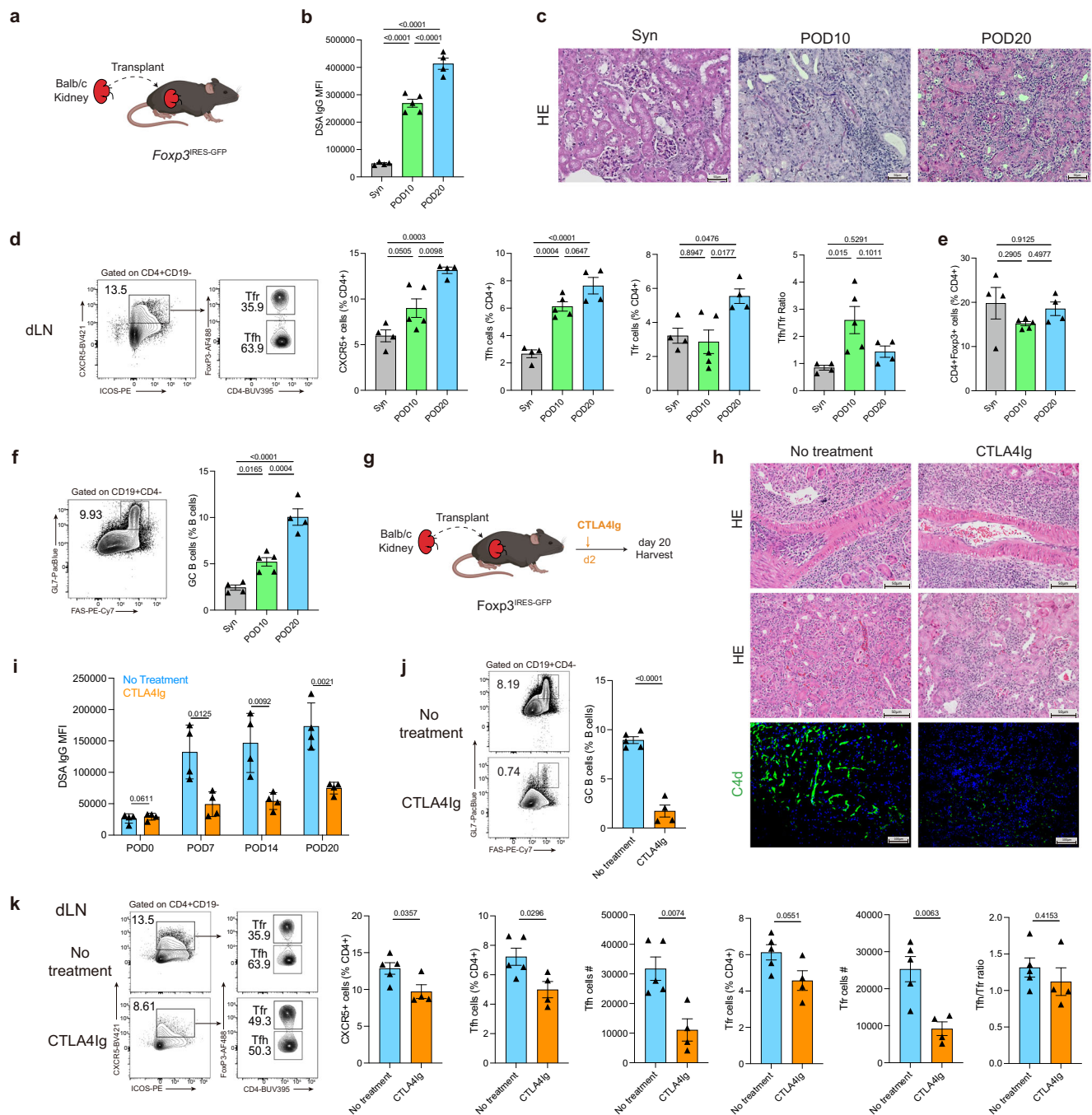
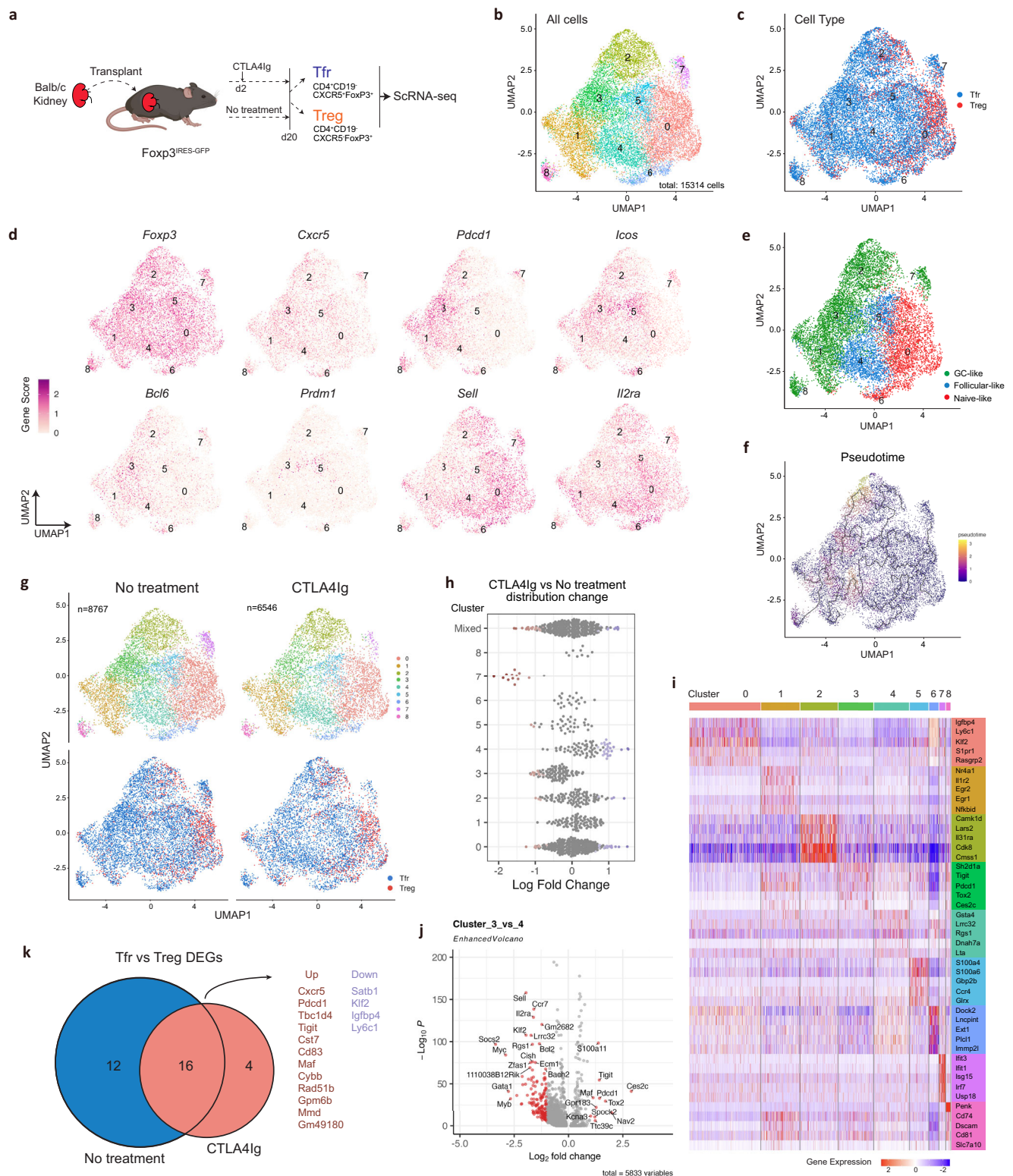


Fig. 1 | Costimulatory blockade dampens Tfr cell differentiation after allogeneic kidney transplantation. **a** Schematic of kidney transplantation. Balb/c (allogeneic) or C57BL/6 (syngeneic) underwent kidney transplantation into *Foxp3^{ires-GFP}* reporter mice. Recipients were harvested 20 days post-transplantation to assess immune response and graft rejection. **b** The levels of DSA IgG in the serum were measured by flow cytometry and presented as MFI ($n = 4$ for the Syn and POD20 group, $n = 5$ for the POD10 group). POD: post-operative day. MFI: mean fluorescence intensity. **c** Representative histological images of kidney grafts at post-operative day 20. Magnification: 200 \times , scale bars: 50 μ m. **d** Gating strategy (left) and quantification (right) of follicular CXCR5⁺ T, Tfh (gated as CD4⁺CD19⁺CXCR5⁺FoxP3⁺), and Tfr (gated as CD4⁺CD19⁺CXCR5⁺FoxP3⁻) cells in the spleen and dLN. $n = 4$ for the Syn and POD20 group, $n = 5$ for the POD10 group. **e** Frequency of CD4⁺FoxP3⁺ Treg cells in total CD4⁺ T cells in the spleen and dLN ($n = 4$ for the Syn and POD20 group, $n = 5$ for the POD10 group). **f** Gating strategy (left) was used to identify and quantify (right) CD19⁺GL7⁺FAS⁺ germinal center (GC) B cells from dLNs. $n = 4$ for the Syn and POD20 group, $n = 5$ for the POD10 group.

g Schematic of CTLA4Ig treatment after kidney transplantation. **h** Representative histological images of transplanted kidneys from CTLA4Ig treated mice are shown, stained with hematoxylin and eosin (HE) (Magnification: 200 \times , scale bars: 50 μ m) and ABMR marker C4d (Magnification: 100 \times , scale bars: 100 μ m). **i** IgG DSA levels at indicated time points from the experiment as in (g). $n = 4$ mice per group. Student's two-tailed unpaired T-test was used to compare two groups. Bonferroni correction was used to control for multiple comparisons. **j** Gating strategy (left) and frequency (right) of GC B cells from dLNs with ($n = 4$) or without CTLA4Ig treatment ($n = 5$). **k** Gating strategy (left) and quantification (right) of follicular CXCR5⁺ T, Tfh (gated as CD4⁺CD19⁺CXCR5⁺FoxP3⁺), and Tfr (gated as CD4⁺CD19⁺CXCR5⁺FoxP3⁻) cells from dLNs ($n = 5$ for the No treatment and $n = 4$ for the CTLA4Ig group). Data is from one experiment and is representative of two independent experiments. Error bars show mean \pm SEM. Student's two-tailed unpaired T test (**j**, **k**), One-way ANOVA with Tukey's multiple-comparison test (**b**, **d**–**f**). Source data are provided as a Source Data file. Portions created in BioRender. Zhang, H. (2025) <https://BioRender.com/b29q775>.



particularly cluster 5. *Pdcd1*/PD-1 was enriched in clusters 1, 3, 7 and 8 which was also largely enriched in *Bcl6*, an important transcription factor for the development and maintenance of Tfh and Tfr cells. Moreover, we found *Il2ra*/CD25 was lowest in *Pdcd1*⁺*Bcl6*⁺ clusters and highest in *Pdcd1*⁺*Prdm1*⁺ Tfr clusters. Since CD25 has been reported to be downregulated in Tfr cells that reside in GCs¹⁷, we have termed clusters 1, 2, 3, 7 and 8, “GC-like” Tfr clusters. Monocle pseudotime analysis indicated a directional progression from naïve-like cluster 0 towards Tfr clusters with *Bcl6* expressing clusters 1,2,3 having higher

pseudotime values compared to *Prdm1*-expressing clusters, except for cluster 7 (Fig. 2f and Supplementary Fig. 4f). In vitro experiments in which we sorted and cultured PD-1⁺ or PD-1⁺ Tfr cells with Tfh and B cells showed that both subsets contained the ability to suppress Tfh-mediated B cell activation, with the PD-1⁺ subset showing a slightly higher inhibitory capacity (Supplementary Fig. 5a). These data indicate that Tfr cells exist in distinct cellular states with unique programming.

Next, we compared how costimulatory blockade altered Tfr cellular states of the cells that were still present after CTLA4Ig treatment.

Fig. 2 | The follicular to GC-like developmental transition in Tfr cells is sensitive to costimulatory blockade. **a** Diagram of single-cell RNA sequencing experiment. Balb/c kidneys were transplanted into *Foxp3*^{RES-GFP} mice with or without CTLA4Ig treatment. Tfr (CD4⁺CXCR5⁺FoxP3⁺) and Treg (CD4⁺CXCR5⁺FoxP3⁺) cells from dLN were sorted and scRNAseq performed. **b** UMAP plot showing unsupervised clustering of all post-filter cells. The total number of cells analyzed is shown. **c** Cells in UMAP plot marked by cell type. **d** Feature plots showing the expression levels of indicated genes of interest across clusters. **e** Clusters annotated based on gene expression states, including Naïve-like, Follicular-like, and GC-like. **f** Monocle pseudotime analysis utilizing cluster 0 as the starting node and indicating developmental trajectories by lines and overall pseudotime by color, plotted within UMAP space. **g** UMAP plot showing clustering (top) and

cell type (bottom) for cells in no treatment or CTLA4Ig treated mice. Number of cells per group is indicated. **h** Cluster distribution changes analyzed with miloR package. Red dots indicate a reduced cell population while blue dots indicate an increased cell population with the CTLA4Ig treatment. **i** Heatmap showing top marker genes for each cluster compared to all clusters. **j** Volcano plot showing differentially expressed genes (DEGs) between clusters 3 and 4. DEGs were identified using a two-sided Wilcoxon rank-sum test, as implemented by the Seurat FindMarkers function (logFC threshold=0.1, min.pct=0.1). *p*-values were adjusted for multiple comparisons using the Bonferroni method. **k** Venn diagram showing differentially expressed genes between Tfr and Treg cells in control or CTLA4Ig treated group. Portions created in BioRender. Zhang, H. (2025) <https://BioRender.com/b29q775>.

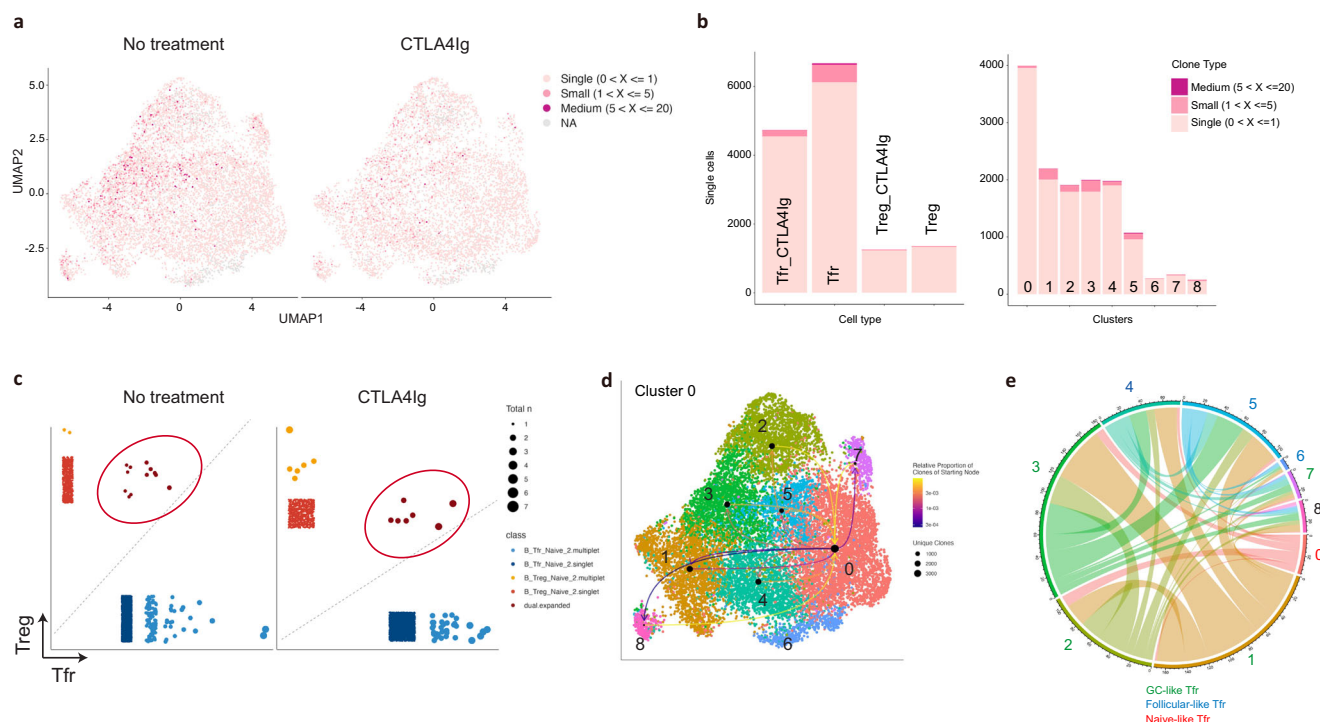


Fig. 3 | Costimulatory blockade restricts Tfr clonal expansion. **a** Clonal expansion indicated in UMAP space utilizing scRepertoire. Each dot represents an individual cell, with colors indicating the size of clonal expansion. Pink indicates singleton clones, while dark pink and red indicate small ($1 < x \leq 5$) and medium ($5 < x \leq 20$) clonal expansion, respectively. **b** Distribution of clonal expansion across experiment groups (left) and clusters (right). **c** Correlation of

clonal expansion and sharing of clones between Tfr and Treg cells calculated by scRepertoire. Circled clones indicate shared clones. **d** Proportion of clonal sharing between cluster 0 and other clusters, with cluster 0 set as founder clones. The thickness of lines indicates magnitude of shared clones. **e** Circos plot showing sharing of expanded clones between clusters. Only expanded clones are included.

We found most Tfr cell clusters remained unchanged except for GC-like Tfr clusters 3 and 7, which were decreased in CTLA4Ig-treated recipients, and follicular-like Tfr cluster 4 which was more abundant in CTLA4Ig-treated recipients (Fig. 2g, h). The enrichment of coinhibitory receptors such as *Tigit*, *Pdcd1* and *Ctla4* in GC-like cluster 3, as well as the enrichment of *Sell*, *Ccr7* and *Il2ra* (CD25) in follicular-like Tfr cluster 4, combined with directional pseudotime analysis suggest CTLA4Ig treatment disproportionately limits the conversion of Tfr cells in the follicular-like state to the GC-like state (Fig. 2i, j). In support of this, these genes were differentially expressed between clusters 3 and 4 (Fig. 2i). Interestingly, the most profoundly affected GC-like cluster by costimulatory blockade was cluster 7 which expressed genes consistent with type-1 interferon responses such as *Ifit3* and *Ifit1* (Fig. 2i). The overall maintenance of core Tfr genes with CTLA4Ig treatment suggested costimulatory blockade did not alter global Tfr programs (Fig. 2k). We identified 12 genes, encompassing *Cxcr5*, *Pdcd1*, *Tbc1d4*, *Tigit*, and *Cst7*, that were significantly upregulated in Tfr vs. Treg cells, and 4 genes - *Satb1*, *Klf2*, *Igfbp4*, and *Ly6c1* - that were markedly downregulated in Tfr vs. Treg cells regardless of whether the Tfr cells

originated from control or CTLA4Ig treated condition (Fig. 2k). Flow cytometry confirmed that naïve-like Tfr cells increased after CTLA4Ig treatment (Supplementary Fig. 5b, c). Together, these data indicate that the Tfr population that develops after solid organ transplantation is phenotypically heterogeneous and that costimulatory blockade disproportionately impedes GC-like Tfr cells compared to other Tfr cell populations.

To assess clonal dynamics of Tfr cells after costimulatory blockade, TCR sequences from the scRNAseq dataset were analyzed. In control recipients, clonal expansion was found mostly in *Bcl6*-expressing GC-like Tfr clusters 1, 2 and 3 and to a lesser extent in *Prdm1*-expressing follicular-like cluster 5 (Fig. 3a, b). CTLA4Ig treatment diminished the extent of clonal expansion in Tfr cells, but not Treg cells, which showed little clonal expansion. To assess the possibility of Treg cell clones differentiating into Tfr cells, we assessed clonal overlap between these compartments. We found similar shared clones between Treg and Tfr cells for both control and CTLA4Ig treated recipients (Fig. 3c). To confirm that cells from naïve-cluster 0 could develop into other cell states, we performed clonal sharing analysis

starting with cluster 0 as the clonal origin. We found shared clones with cluster 0 for both GC and follicular-like Tfr clusters (Fig. 3d). Clonal sharing of expanded clones between clusters showed substantial sharing within and between follicular-like and GC-like Tfr clusters (Fig. 3e). Together, these data elucidate developmental trajectories of Tfr cells from a naïve state, through a follicular-like state and ultimately into an activated GC-like state after kidney transplantation and that costimulatory blockade disproportionately inhibits the GC-like state and clonal expansion of Tfr cells.

Tfr cells limit allo-antibody production and rejection of kidney allografts

To elucidate the precise roles of Tfr cells in the context of kidney allograft rejection, we utilized a previously described intersectional genetics-based Tfr-deleter (Tfr-DTR) mouse model that selectively eliminates Tfr cells with administration of diphtheria toxin (DT)^{18,19,27}. This strain harbors both a *Cxcr5*^{LoxSTOPLoxDTR} allele and a *Foxp3*^{CreYFP} allele, positing DTR on the surface of Tfr cells but not other follicular T, nor Treg, cells. We performed allogeneic kidney transplantation to control (Tfr-Con; *Foxp3*^{CreYFP}*Cxcr5*^{WT}) or Tfr-DTR (*Foxp3*^{CreYFP}*Cxcr5*^{LoxSTOPLoxDTR}) mice and administered a single dose of CTLA4Ig on day 2 to lengthen the time of rejection, thereby facilitating a more complete understanding of Tfr functions (Fig. 4a). In survival transplant models (where recipient native kidneys were rendered non-functional via bilateral ureter obstruction so that the transplanted organ sustains the life of the recipient), Tfr cell deletion starting on day 3 reduced recipient survival time to 25 ± 5.04 days, in contrast to the median survival of 60 ± 20.08 days observed in the Tfr-Con group, and 20 ± 1.79 days without any treatment (Fig. 4b). At 20 days post-transplantation (utilizing mechanistically similar non-survival transplant surgeries), Tfr-deleted mice displayed significantly enlarged grafts and spleens, characterized by increased GC structures (Fig. 4c and Supplementary Fig. 6a). Both Tfr deleted and sufficient groups exhibited similarly high levels of TCMR-like pathological features, including tubulitis, arteritis, and interstitial inflammation. In non-deleted control mice, mononuclear cells were primarily localized to the renal interstitium and around arteries. In contrast, in Tfr-deleted mice, the infiltrates were more diffusely distributed across glomeruli, tubules, and peritubular capillaries (Fig. 4d and Supplementary Fig. 6b, c). There was also evidence of thrombotic microangiopathy and substantial C4d deposition (Fig. 4d and Supplementary Fig. 6b, c). Together, these parameters indicate more severe ABMR-like disease in Tfr-deleted mice. These findings also suggest that Tfr cells regulate ABMR-like disease processes more substantially than TCMR-like processes. Additionally, although CD4⁺ and CD8⁺ T cell infiltration remained largely unchanged, CD68⁺ macrophage infiltration was significantly enhanced in Tfr-deleted mice (Supplementary Fig. 6d). While the overall B cell infiltration in Tfr-deleted recipients was equal or even reduced compared to control recipients, local IgG deposition was increased (Fig. 4d).

Deletion of Tfr cells did not alter the serum levels of IL-2 and IFN- γ production (Supplementary Fig. 6e). Serological analyses of DSA indicated that total IgG DSA levels began increasing from day 14 and showed a three-fold increase in Tfr-DTR, compared to control, recipients by day 20 after transplantation (Fig. 4e and Supplementary Fig. 6f). When we assessed individual allo-epitopes using single antigen beads, we found a pronounced elevation in IgG antibodies targeting MHC-Class II (I-A^d and I-E^d) antigens in the absence of Tfr cells (Fig. 4f). We and others have previously shown that deletion/perturbation of Tfr cells results in increases in autoreactive antibodies^{18,31}. Therefore, we next assessed autoreactive antibodies using a Hep-2 antibody detection assay with subcellular distribution assessment³². We observed heightened autoreactive antibodies from Tfr-deleted compared to control mice and these antibodies recognized cytoplasmic and nuclear targets (Fig. 4g). Together, our data demonstrate that Tfr cells have potent roles in limiting features of ABMR and promoting recipient

survival after allogeneic kidney transplantation by controlling both donor-specific and autoreactive antibody responses.

Tfr cells restrain lymph node and intragraft GC B cell development

Next, we examined the role of Tfr cells in controlling GC B cell responses (Fig. 5a). We and others have previously shown that pathogenic GC-like B cells can be present in both lymph nodes and kidney allografts^{2,25}. In the dLN after transplantation, a marked reduction in Tfr, but not total Treg nor non-Tfr Treg cells, was observed in Tfr-DTR recipients validating specificity of deletion (Fig. 5b and Supplementary Fig. 7a, b). The frequency and total number of Tfh cells (gated as CD4⁺CXCR5⁺Foxp3⁺) in the dLN, but not the blood (Supplementary Fig. 7c), increased with Tfr deletion suggesting Tfh cells are restrained by Tfr cells after transplantation, a finding that has been reported during vaccine settings^{18,33}. Compared to Tfr-sufficient control mice, Tfr cell deletion culminated in a significant augmentation in the frequency of GC B, memory-like B, and total IgG⁺ B cells in the dLN (Fig. 5c, d). Conversely, there was a notable decline in the naïve B cell (gated as CD19⁺CD38⁺IgG1⁺) population in Tfr-deleted mice. Within the allograft, the Tfr cell frequency and cell numbers mirrored the observations in dLN, with a substantial attenuation in Tfr-DTR mice (Fig. 5e and Supplementary Fig. 7d). Previous studies have shown that kidney allograft infiltrating B cells have a GC-like phenotype marked by GL7 expression even though they transcriptionally resemble innate-like B cells^{2,32}. We found the frequency and total number of intragraft GL7⁺ B cells increased in the absence of Tfr cells compared to Tfr sufficient controls (Fig. 5f and Supplementary Fig. 7d). Together, these data demonstrate that Tfr cells significantly restrain GC-like B cell responses simultaneously in dLNs as well as in kidney allografts.

Tfr cells restrict pathogenic B responses within lymph nodes and grafts

To understand the role of Tfr cells in controlling alloreactive GC B cells that produce pathogenic antibodies in lymph nodes and grafts we performed a GC single-cell culture system which allows interrogation of antigen specificity at a clonal level utilizing highly sensitive ELISA assays to assess broad alloreactivity (Fig. 5g)^{2,25}. For this, individual GL7⁺ B cells from dLN or kidney allografts from allogeneic transplant recipients on day 20 after transplantation were cultured with NB21 feeder cells allowing expansion and antibody secretion¹⁹. Culture supernatants were screened for IgG positivity by ELISA and IgG⁺ clones were further screened for alloreactivity (Fig. 5h). We found ~40% of IgG⁺ GC B cells from the dLN were donor-specific in control transplant recipients. This increased to ~46% in recipients in which Tfr cells were deleted starting on day 3 post-transplant, further compounding the already 3-fold increase in the frequency of total GC B cells (Fig. 5i, c). We have previously shown that although intragraft GC-like B cells are rarely class-switched, the few IgG⁺GL7⁺ B cells in grafts can be alloreactive². Consistent with this, we found that ~42% of IgG⁺GL7⁺ B cells in allografts of transplanted Tfr-sufficient recipients were specific for alloantigen. In Tfr-deleted recipients, this increased to ~50%, although the difference did not reach statistical significance. Together these data indicate that Tfr cells not only control the frequency of GC-like B cells but also the proportion of pathogenic alloreactive B cell clones within these compartments in both lymph nodes and kidney allografts.

Intensified B cell alloimmunity after Tfr cell deletion does not require CD8 T cells

We next assessed whether CD8 T cells were required for the intensified rejection which occurred after Tfr cell deletion. To do this, we administered a CD8-depleting antibody to control and Tfr-DTR mice and assessed B cell alloimmunity and graft pathology (Fig. 6a). Flow cytometry and immunohistochemistry confirmed a marked reduction in

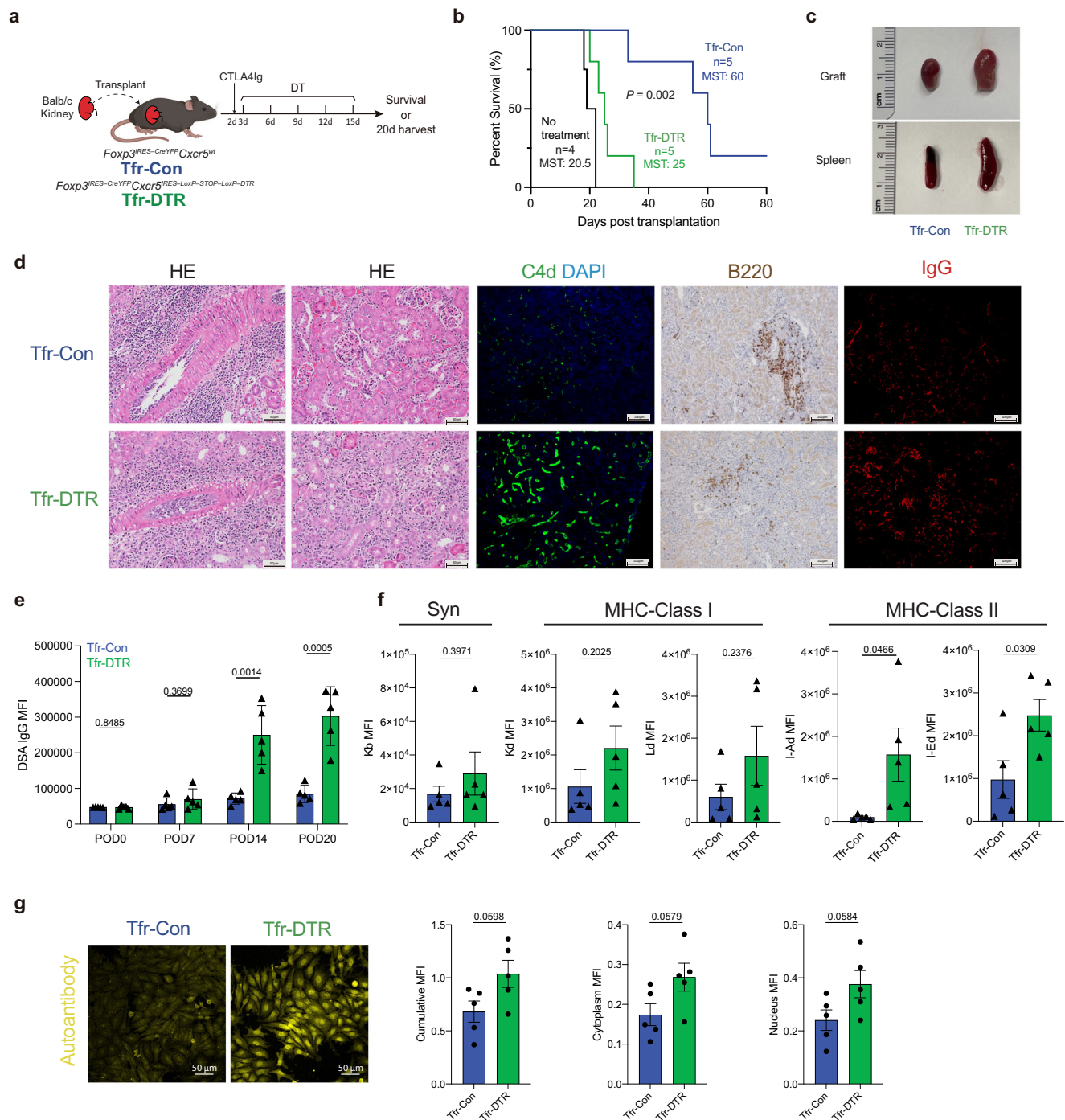
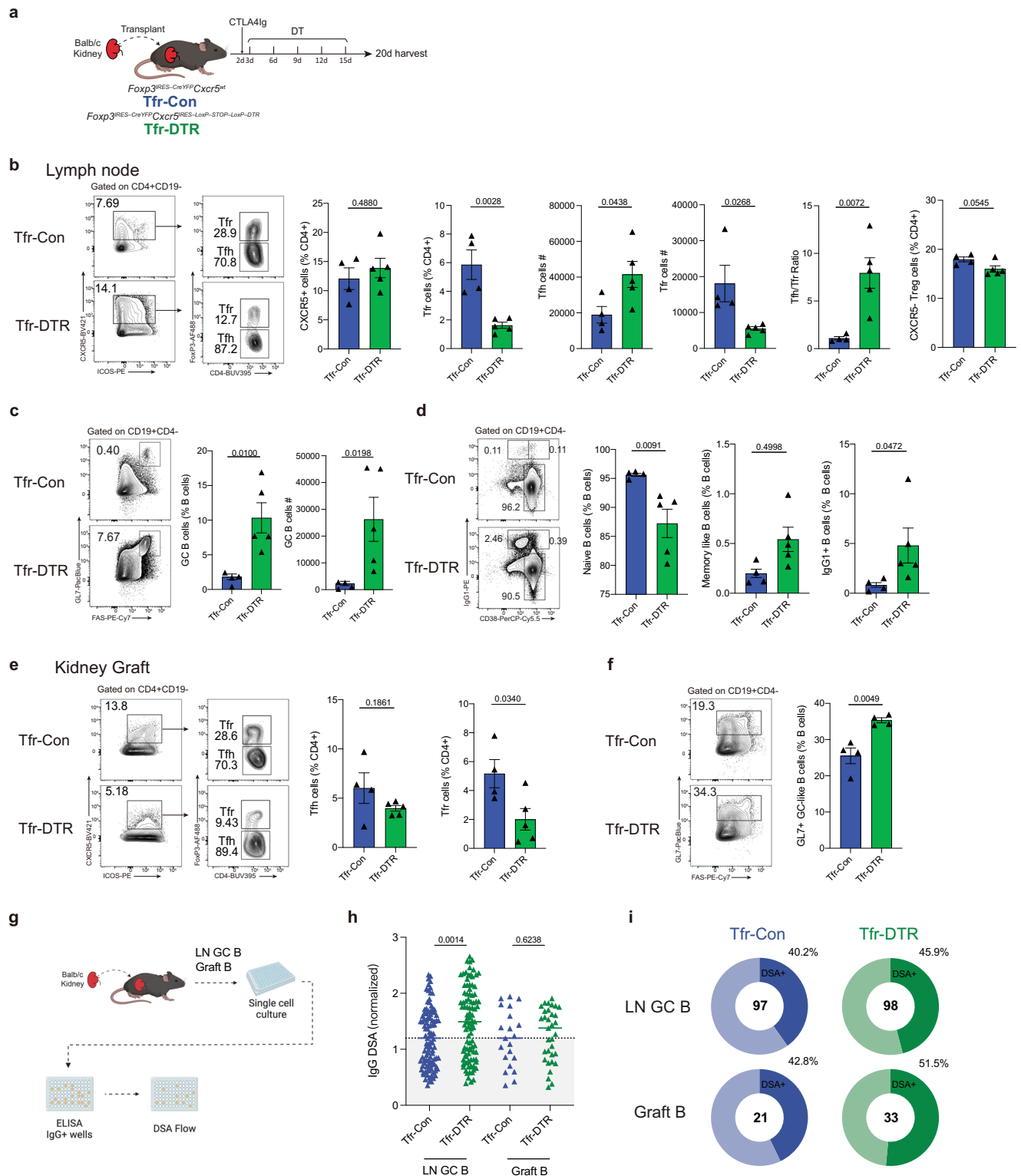


Fig. 4 | Tfr cells prevent allo-antibody formation and rejection of kidney allografts. **a** Schematic of Tfr cell deletion using Tfr-DTR mice. Control (Tfr-Con, *Foxp3^{CreYFP}Cxcr5^{fl}*) or Tfr-DTR (*Foxp3^{CreYFP}Cxcr5^{fl}STOP-LoxP-DTR*) mice received diphtheria toxin (DT), CTLA4Ig (on day 2) and Balb/c kidneys as life-sustaining (b) or non-life-sustaining (c–g) transplants. **b** Survival of transplanted recipients not receiving CTLA4Ig (no-treatment), or CTLA4Ig treated Tfr-Con or Tfr-DTR mice. MST, median survival time. **c** Spleens and kidney grafts from Tfr-Con and Tfr-DTR mice harvested 20 days after transplantation. **d** Representative histological images of kidney grafts at postoperative day 20, including hematoxylin and eosin (HE), immunohistochemistry staining for B220, and immunofluorescence staining for C4d and IgG. Scale bars: 50 and 100 μ m. **e** IgG DSA levels in serum at indicated time points.

MFI=mean fluorescence intensity. $n = 5$ mice per group. **f** Allo-reactive IgG to individual MHC molecules measured by single antigen bead. Syn= syngeneic. $n = 5$ mice per group. **g** Quantification of serum autoantibody levels. Representative images of serum from mice as in (a) incubated with Hep-2 cells (left) and quantification of cumulative, cytoplasm, and nucleus antibody signal. $n = 5$ mice per group. Scale bars: 50 μ m. Data is from one experiment and is representative of two independent experiments. Statistics: Error bars show mean \pm SEM. Student's two-tailed unpaired T test for 2-group comparisons and Kaplan-Meier survival analysis and a log-rank test for survival analysis (b). Source data are provided as a Source Data file. Portions created in BioRender. Zhang, H. (2025) <https://BioRender.com/b29q775>.

CD8⁺ T cells in both the dLN and grafts of anti-CD8 treated recipients without significant changes in the populations of CD44⁺CD62L⁺ effector CD4⁺ T cells or CD69⁺ activated effector CD4⁺ T cells (Supplementary Fig. 8a–e). Moreover, Tfr cell deletion occurred normally

(Supplementary Fig. 8f). IgG DSA levels increased in the serum of Tfr-deleted, compared to control, mice as did GC B cells and IgG1⁺ GC B cells in both the dLN and grafts (Fig. 6b–d and Supplementary Fig. 8g). Despite effective CD8⁺ T cell depletion, histological analysis revealed



interstitial cellular infiltration in both groups, with no significant differences in TCMR-like pathological scoring (Fig. 6e and Supplementary Fig. 8h). T cell-related cytokines IL-2 and IFN- γ in the serum also showed no significant differences with the deletion of Tfr cells (Supplementary Fig. 8i). The intensified B cell responses and number of GCB cells in the graft also correlated with increased glomerulitis, peritubular capillaritis and C4d deposition in the grafts of Tfr deleted, compared to control, mice (Fig. 6e and Supplementary Fig. 8j, k). These findings suggest that the intensified B cell alloimmunity and

ABMR-like disease that occurs after Tfr deletion does not require CD8 T cells.

To confirm whether the increased DSA in Tfr-deleted mice was sufficient to induce ABMR-like disease we conducted passive transfer experiments. We collected serum from kidney transplanted control or Tfr-DTR recipients (performed as in Fig. 4). Serum was transferred to kidney transplanted μ MT (*Ighm*^{-/-}) mice that lack most mature B cells and therefore cannot produce DSA (Fig. 6f). The transplanted μ MT recipients that received serum from Tfr-DTR mice showed significantly

Fig. 5 | Tfr cells restrain lymph node and intra-graft germinal center B cell differentiation. **a** Schematic of Tfr cell deletion using Tfr-DTR mice. Tfr-Con (*Foxp3^{CreYFP}Cxcr5^{wt}*) or Tfr-DTR (*Foxp3^{CreYFP}Cxcr5^{LoxSTOPLoxTfr}*) mice received diphtheria toxin (DT), CTLA4Ig (on day 2) and Balb/c kidneys. **b** Gating strategy and quantification of CXCR5⁺ follicular T, Tfh (gated as CD4⁺CD19⁺CXCR5⁺FoxP3⁺), Tfr (gated as CD4⁺CD19⁺CXCR5⁺FoxP3⁺), and CXCR5⁺FoxP3⁺ T cells in total CD4⁺ T cells from the dLNs. *n* = 4 mice for the Tfr-Con group and *n* = 5 for the Tfr-DTR group. **c** Gating strategy (left) and quantification (right) of CD19⁺GL7⁺FAS⁺ GC B cells. *n* = 4 mice for the Tfr-Con group and *n* = 5 for the Tfr-DTR group. **d** Gating strategy (left) and quantification (right) of Naïve B cells (CD38⁺IgG1⁺CD19⁺), memory-like B cells (CD38⁺IgG1⁺CD19⁺), and IgG1⁺ B cells in the dLN (*n* = 4 for Tfr-Con and *n* = 5 for Tfr-DTR). **e** Gating strategy and quantification of Tfh and Tfr cells in kidney allografts (*n* = 4 for Tfr-Con and *n* = 5 for Tfr-DTR). **f** Gating strategy and quantification of GC-

like B cells (GL7⁺CD19⁺) in kidney allografts. *n* = 4 mice for each group. **g** Schematic of GC B single cell culture assays. Single GC B cells from dLN or grafts were sorted and cultured with NB21 feeder cells for 6 days. Culture supernatants were pre-screened for IgG positivity and further assessed for DSA reactivity. **h** DSA signal of individual IgG⁺ clones from LN GC B and graft B cells from either control or Tfr-DTR mice 20 days after transplantation. The dotted line indicates the level of detection threshold assessed by signal using syngeneic cells. **i** Frequency of DSA clones (from all IgG⁺ clones). Numbers indicate the total number of IgG clones analyzed. Data is from one experiment and is representative of two independent experiments. Statistics: Error bars show mean ± SEM. Student's two-tailed unpaired T test for 2-group comparisons. Source data are provided as a Source Data file. Portions created in BioRender. Zhang, H. (2025) <https://BioRender.com/b29q775>.

higher IgG and C4d deposition in kidney grafts compared to those that received serum from control mice (Fig. 6g). These findings suggest that the alloantibodies produced after Tfr cell deletion contribute to disease.

Tfr cells fail to control the later stages of ABMR after kidney transplantation

Previous studies have demonstrated that Tfr cells have more potent roles in controlling early GC responses but have less substantial roles after GC formation¹⁸. To further understand the role of Tfr cells in controlling later stages of ABMR after kidney transplantation, we transplanted allogeneic kidneys into Tfr-DTR or control mice, gave CTLA4Ig on day 2, and administered DT to delete Tfr cells starting on day 20, a timepoint during which the rejection process is already underway. We evaluated B cell alloimmunity on day 30 (Fig. 7a). Tfr-DTR mice had similar IgG DSA as control mice suggesting Tfr cells did not restrain pathogenic antibody after GC formation (Fig. 7b and Supplementary Fig. 9a). By day 30 post-transplantation, grafts from both Tfr sufficient and deleted groups showed similar signs of rejection including mononuclear cell infiltration and pathological features of ABMR (Fig. 7c). As expected, a marked reduction in Tfr cells was observed in the Tfr-DTR mice, while the frequencies and number of Tfh and other naïve Treg cells remained unchanged (Fig. 7d and Supplementary Fig. S9b). Consistent with the lack of changes in the Tfh compartment, we did not find any substantial differences in the percentage and number of GC B cells in lymph nodes between Tfr-DTR and control mice (Fig. 7e and Supplementary Fig. 9c). Moreover, we did not find any differences in the frequencies of naïve B cells, IgG1 or IgG2-switched B cells, nor memory-like B cells when Tfr cells were deleted starting at day 20 (Fig. 7e, f). These data demonstrate that Tfr cells have strong roles in restraining ABMR early after kidney transplantation but are unable to dampen ongoing ABMR.

Tfr cells control kidney transplant rejection by restraining proinflammatory cytokines in GC B cells

To uncover mechanisms by which Tfr cells control rejection after kidney transplantation, we isolated LN GC B cells from control or Tfr-DTR recipients 20 days post-transplantation and performed bulk RNAseq transcriptional analyses (Fig. 8a). Our analysis identified 662 differentially expressed genes (*p* < 0.05), with 275 genes exhibiting increased expression in Tfr-deleted recipients (Fig. 8b). KEGG pathway analysis indicated that differentially expressed genes were enriched in pathways such as cytokine-cytokine receptor interaction, MAPK, TNF, and JAK-STAT signaling (Fig. 8c). In the cytokine pathway, *IL15* transcripts were found to be upregulated in GC B cells from Tfr-DTR mice compared to Tfr-Con mice (Fig. 8b). IL-15 is a pleiotropic cytokine that activates T and NK cells and has roles in promoting B cell responses by enhancing Tfh cells^{34–36}. To validate Tfr cells control IL-15 protein levels, we compared IL-15 concentrations in dLN interstitial fluid by ELISA. The concentration of IL-15 was elevated in Tfr-DTR compared to control recipients (Fig. 8d). Flow cytometry further confirmed a minor

increase in IL-15 and IL15ra expression in dLN GC B cells in the absence of Tfr cells (Supplementary Fig. 10a, b).

To assess the potential roles of increased IL-15 in promoting pathogenic B cell responses, we performed an in vitro functional assay where Tfh and Tfr cells, isolated from allogeneic kidney transplantation recipients, were co-cultured with B cells in the presence of anti-CD3/IgM (Fig. 8e)^{2,25}. Tfh cells cultured with B cells resulted in increases in IL-15 in culture supernatants and addition of Tfr cells reduced IL-15 levels significantly (Fig. 8f). To specifically assess the impact of IL-15 on B cell responses, we introduced a blocking antibody to neutralize IL-15. Tfh cells stimulated approximately 50% of B cells to express the activation marker GL7 which was substantially reduced when IL-15 was blocked (Fig. 8g and Supplementary Fig. 10c). In addition, while anti-IL-15 treatment dampened Tfh-induced IgG production by B cells, it did not further amplify the inhibitory effect of Tfr cells (Fig. 8h). Prior single-cell sequencing of Tfh in dLN and grafts of kidney transplantation mice did not show evidence of *Il15* transcript²⁵ (Supplementary Fig. 10d). Although myeloid cells in the kidney can produce IL-15, culture of these cells with Tfr cells did not result in any differences in IL-15 secretion (Supplementary Fig. 10e, f). Our findings indicate that IL-15 production by B cells is induced by Tfh cells and inhibited by Tfr cells.

To further investigate the role of IL-15 in rejection, we evaluated the immune response in kidney transplanted IL-15Rα-deficient mice (IL-15Rα KO) (Fig. 8i, j). IL-15Rα KO mice had diminished GC B cell and IgG DSA responses (Fig. 8j and Supplementary Fig. 10g, h). Furthermore, in vitro functional assays in which IL-15Rα KO or control B cells were cultured with Tfh cells demonstrated reduced B cell and Tfh cell activation, indicating that B cells may be capable of trans-presenting IL-15 (Supplementary Fig. 10i–l). To confirm that IL-15 could be sensed by Tfh cells, we cultured Tfh cells sorted from the dLN of transplant recipients with IL-15 for 6 h and performed bulk RNA sequencing (Supplementary Fig. 10m, n). Transcriptomic analysis revealed that IL-15-stimulated Tfh cells exhibited a transcriptional profile consistent with enhanced activation and metabolic reprogramming (Supplementary Fig. 10o–q).

To assess the roles of IL-15 in the intensified ABMR-like disease in Tfr-deleted mice we neutralized IL-15 in vivo after Tfr deletion in transplanted mice receiving costimulatory blockade (Fig. 8k). Tfr-DTR recipients treated with both DT and anti-IL-15 neutralizing antibodies had increased survival compared to control Tfr-DTR mice that received DT alone (Fig. 8l). At 20 days post-transplantation, the anti-IL-15 treatment resulted in reduced GC B cells and serological IgG DSA production in Tfr-deleted mice (Fig. 8m and Supplementary Fig. 11a). IL-15 blockade did not significantly alter the frequency of Tfh/Tfr cells in dLN, IL-2 and IFN-γ production in the serum, nor infiltration of T cells/ MHC class II+ cells in the grafts (Supplementary Fig. 11b–d). IL-15 blockade alone in the presence of normal Tfr cells did not significantly diminish germinal center B cell responses nor DSA levels (Supplementary Fig. 11e, f). In contrast to kidney transplantation settings, anti-IL-15 treatment did not significantly suppress GC B cells nor

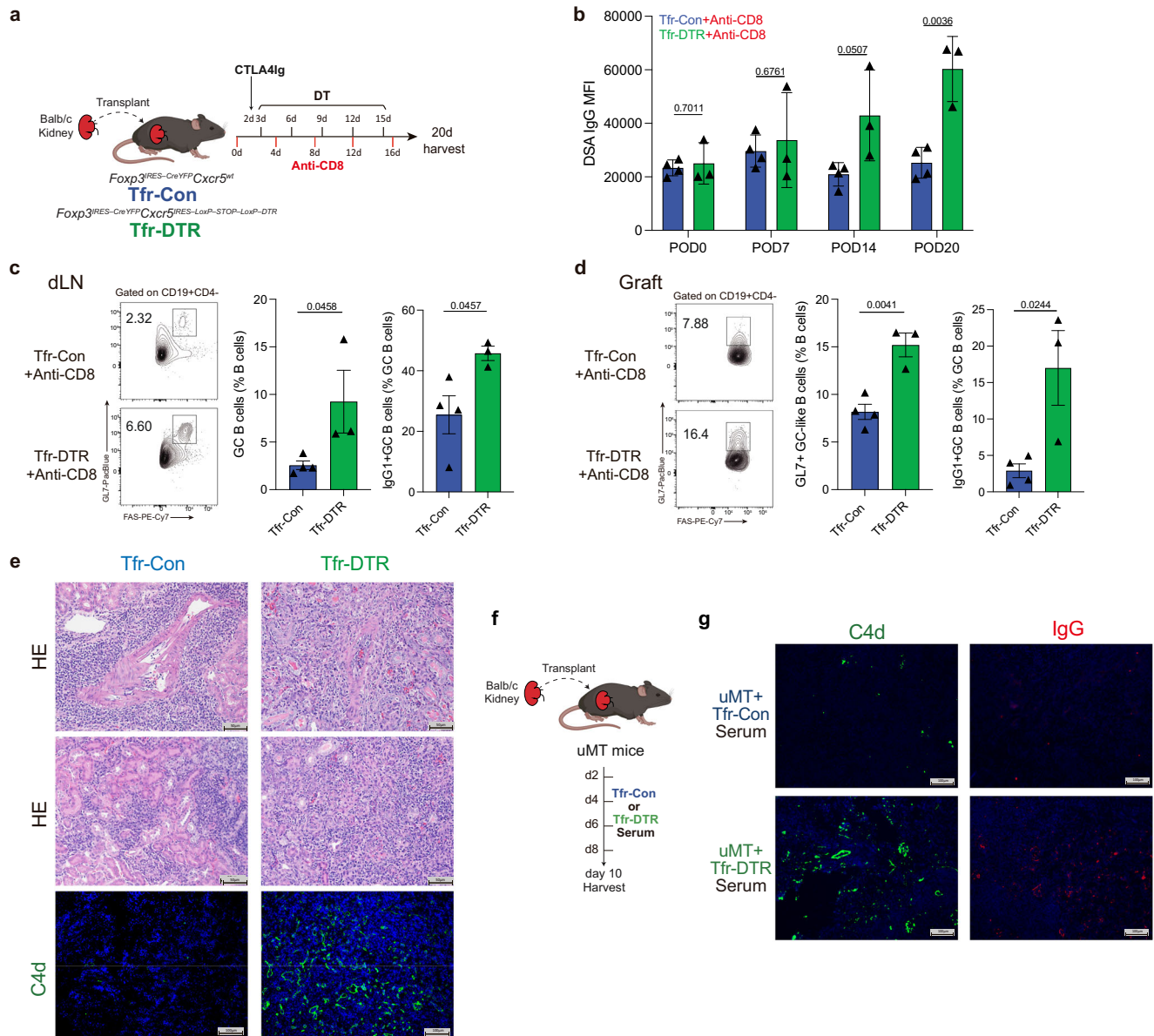


Fig. 6 | Intensified graft rejection after Tfr cell deletion does not require CD8 T cells. **a** Schematic of experiment for which Tfr-Con or Tfr-DTR mice were administered a CD8 depleting antibody, CTLA4Ig, and diphtheria toxin (DT) to delete Tfr cells. Organs were harvested on day 20. **b** IgG DSA levels in the serum of Tfr-Con ($n = 4$) and Tfr-DTR ($n = 3$) mice from (a) at indicated time points (POD = post operative day). **c** Representative gating strategy and quantification of GL7⁺FAS⁺ GC B cells and IgG1⁺ GC B cells in dLNs of Tfr-Con ($n = 4$) and Tfr-DTR ($n = 3$) mice. **d** Representative gating strategy and quantification of GL7⁺ B cells in kidney grafts ($n = 4$ for Tfr-Con and $n = 3$ for Tfr-DTR). **e** Representative images of kidney grafts stained with HE (Magnification: 200 \times) or C4d (Magnification: 100 \times)

for Tfr-Con and Tfr-DTR mice. **f** Schematic of assay to assess the ability of DSA from Tfr-Con or Tfr-DTR to mediate C4d deposition. B cell-deficient (μ MT) mice were transplanted with a Balb/c kidney and serum from Tfr-Con or Tfr-DTR mice from (a) were passively transferred. Transplanted graft was harvested on day 10. **g** Representative images showing C4d and IgG deposition in kidney grafts from μ MT mice as in (f). Magnification: 100 \times , scale bars: 100 μ m. Data are combined from two independent experiments. Statistics: Error bars show mean \pm SEM. Student's two-tailed unpaired T test for 2-group comparisons. Source data are provided as a Source Data file. Portions created in BioRender. Zhang, H. (2025) <https://BioRender.com/b29q775>.

antigen-specific IgG in the context of NP-OVA vaccination of Tfr deleted mice, indicating the IL-15 pathway may be unique to transplantation (Supplementary Fig. 11g). Collectively, our findings indicate that Tfr cells potentially restrain rejection after kidney transplantation by limiting alloreactive B cell responses (Fig. 8n).

Discussion

Organ transplantation, a transformative therapeutic intervention for end-stage organ failure, is continually challenged by occurrences of ABMR³⁷. Although the roles of Tfh cells in promoting DSA and ABMR after solid organ transplantation have been studied, the functions of Tfr

cells are less understood due to a lack of mouse models to investigate the precise roles of these cells in vivo. In kidney transplant patients, previous research has established an inverse correlation between the absolute number of circulating Tfr cells and the incidence of ABMR²⁶. Our study identified dynamics of Tfr cell differentiation after kidney transplantation, which occurred alongside the progression of ABMR-like disease. Tfr cells existed in distinct phenotypic states including naïve-like, follicular-like and activated GC-like Tfr cells with the naïve-like Tfr cells overlapping substantially with conventional Treg cells. The core Tfr program is characterized by the upregulation of key genes including *Cxcr5*, *Pdcd1*/PD-1, and *Tigit* compared to conventional Treg cells.

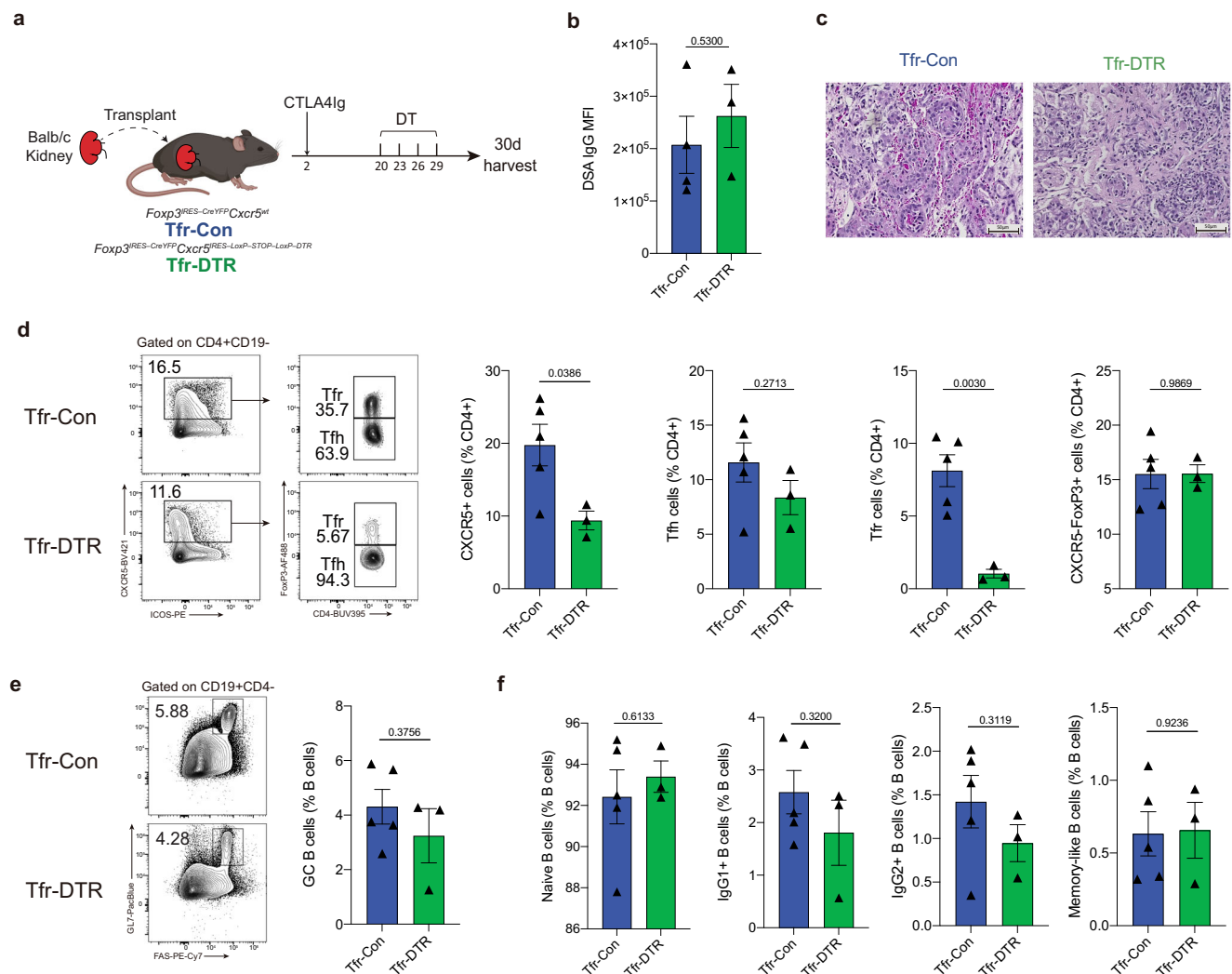


Fig. 7 | Tfr cells fail to control the later stages of rejection after kidney transplantation. **a** Schematic of late Tfr cell deletion after allogeneic kidney transplantation. Tfr-Con or Tfr-DTR mice received Balb/c kidney transplants followed by CTLA4Ig treatment. Diphtheria toxin (DT) was administered starting on day 20 to induce Tfr cell deletion, and mice were analyzed 30 days post-transplantation. **b** Measurement of IgG DSA in the serum of Tfr-Con ($n = 4$) and Tfr-DTR ($n = 3$) mice at 30 days post-transplantation. **c** Pathology of transplanted kidneys using hematoxylin and eosin (HE) staining. Magnification: 200 \times , scale bars: 50 μ m. **d** Gating strategy and quantification of CXCR5⁺ follicular, Tfh, Tfr,

and CXCR5-FoxP3⁺ T cells in total CD4⁺ T cells from the dLNs of Tfr-Con ($n = 5$) and Tfr-DTR ($n = 3$) mice. **e** Gating strategy (left) and quantification (right) of GC B cells ($n = 5$ for Tfr-Con and $n = 3$ for Tfr-DTR). **f** Frequency of Naive (CD38⁺IgG1⁺), IgG1⁺, IgG2⁺ and memory-like (CD38⁺IgG1⁺) B cells in total B cells from the dLN ($n = 5$ for Tfr-Con and $n = 3$ for Tfr-DTR). Data are combined from two independent experiments. Statistics: Error bars show mean \pm SEM. Student's two-tailed unpaired T test for 2-group comparisons. Source data are provided as a Source Data file. Portions created in BioRender. Zhang, H. (2025) <https://BioRender.com/b29q775>.

Previous studies have shown that interfering with PD1-PDL1 interactions early in mouse kidney transplantation leads to increased acute rejection³⁸. Another study demonstrated that activating the TIGIT pathway enhances the suppressive effects of FoxP3⁺ Treg cells on human memory T cell population³⁹. Consistent with our findings, Tfr cells begin exerting regulatory and inhibitory effects early post-transplantation, commensurate with upregulation of PD1 and TIGIT.

Beyond a general Tfr program, we also uncovered unique Tfr cell states with overlapping clonality indicating that Tfr cells differentiate from a naïve-like state, through a “follicular-like” state and into an activated GC-like state. Importantly, this nomenclature refers to activation states (and not anatomical location) and were identified by altered expression of PD-1 and CD25, which have been shown to correlate with presence or absence on Tfr cells in GCs, respectively¹⁷. Importantly, both follicular-like and GC-like Tfr cells had suppressive capacity. Therefore, Tfr cells may require sequential developmental stages to achieve full differentiation, similar to what has been recently shown for Tfh cells³³.

However, additional studies need to be performed to determine the etiology and function of these putative developmental stages.

There have been few, if any, therapeutics developed that limit ABMR. While CTLA4Ig treatment has shown improved graft survival and kidney function compared to calcineurin inhibitors, its association with a higher incidence of acute cellular rejection prevents broad usage^{40–42}. Multiple studies indicate that CTLA4Ig compromises the suppressive function of Treg⁴³. Interestingly, we found that costimulatory blockade strategies inhibited the differentiation of Tfr cells, but did so disproportionately, resulting in diminished GC-like and interferon-responsive Tfr cells. The GC-like Tfr cluster 3 was characterized by the expression of genes like *Sh2d1a*, *Tigit*, and *Pdcd1*. Agonism of TIGIT was observed to enhance Treg function, which was suppressed by CTLA4Ig, in skin transplantation⁴⁴. Therefore, co-administering agents that promote GC-like Tfr differentiation alongside CTLA4Ig may retain the clinical benefits of CTLA4Ig without compromising Tfr function. Additionally, while the use of CTLA4Ig in

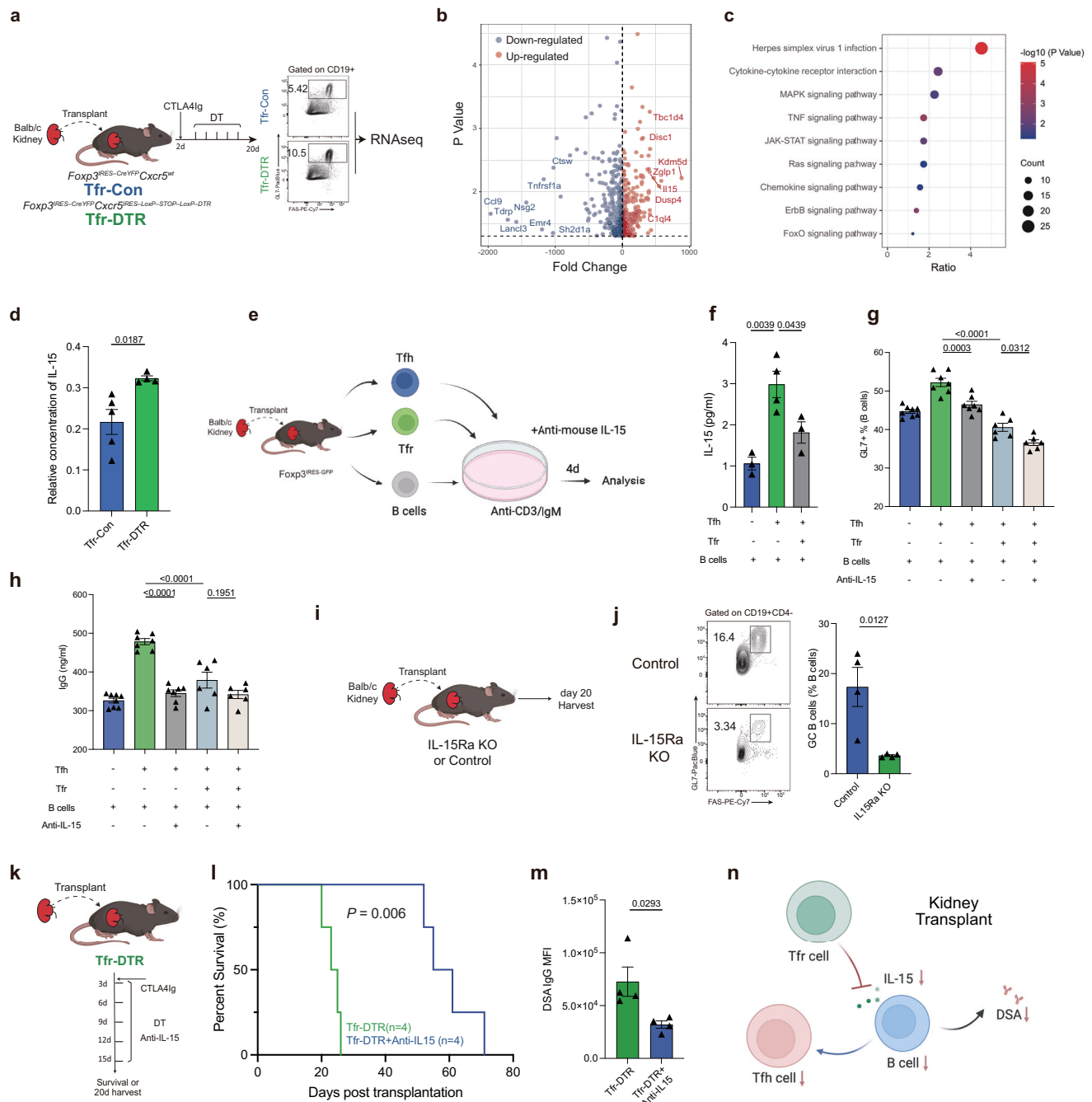


Fig. 8 | Tfr cells dampen transplant rejection by limiting B cell production of IL-15. **a** Diagram of bulk RNAseq experiment. CD19⁺GL7⁺FAS⁺ GC B cells from dLN were sorted from CTLA4Ig and DT treated Tfr-Con or Tfr-DTR recipients and RNAseq performed. **b** Volcano plot indicating differentially expressed genes (DEGs) between Tfr-Con and Tfr-DTR GC B cells as in (a). Genes with a P value < 0.05 are shown highlighted as upregulated (red) or downregulated (blue) in Tfr-DTR. **c** KEGG pathways associated with DEGs from (b). **d** Concentration of IL-15 from interstitial fluid of dLNs from Tfr-Con ($n=5$) and Tfr-DTR ($n=4$) mice, expressed as a relative value to protein concentration. **e** Schematic of in vitro Tfh-mediated B cell stimulation assay. Tfh, Tfr, and B cells from transplant recipients were cocultured for 4 days with anti-CD3/IgM in the presence or absence of 100 ng/ml anti-IL-15. **f** Quantification of IL-15 levels in the supernatant from the co-culture assay described in (e). **g** Percentage of GL7⁺ B cells in the presence of Tfh cells under indicated co-culture conditions. **h** Quantification of IgG in the culture supernatants from culture conditions. **i** Schematic of experiment to assess the role of IL-15 α in B cell alloimmunity after kidney transplantation. IL-15 α KO ($Il15ra^{-/-}$) or control mice received Balb/c kidney

transplants, and grafts were harvested on day 20 for analysis, $n=4$ per group. **j** Gating strategy (left) and quantification (right) of GL7⁺ GC B cells in the dLNs as in (i). $n=4$ per group. **k** Schematic of experiment to assess contribution of IL-15 to exacerbated rejection after Tfr-deletion. Tfr-DTR mice underwent Balb/c kidney transplantation and received CTLA4Ig and DT. Some mice further received anti-IL-15. Mice were either followed for survival or organs harvested on day 20 post-transplantation for analysis. **l** Kaplan-Meier survival curve of transplanted Tfr-DTR recipients with or without anti-IL-15 treatment as in (k). $P = 0.006$. **m** Total IgG DSA from the serum of mice as in (k) 20 days after transplantation. $n=4$ per group. **n** Model summarizing Tfr role in controlling kidney transplant rejection. Red arrow indicates effect of Tfr cells. (a-c, i, j) Data is combined from two experiments. (d-h, k-m) Data is from two experiments and is representative of two independent experiments. Statistics: Error bars show mean \pm SEM. Student's two-tailed unpaired T test (d, j, m), One-way ANOVA with Tukey's multiple comparison test for f-h. Kaplan-Meier survival analysis, and a log-rank test for survival analysis (l). Source data are provided as a Source Data file. Portions created in BioRender. Zhang, H. (2025) <https://BioRender.com/b29q775>.

this study provided a valuable approach to prolong allograft rejection facilitating downstream mechanistic studies on Tfr functions, it is important to note that only a small percentage of kidney transplant patients receive CTLA4Ig.

The roles of Tfr cells in disease progression can be multifaceted and complex. While Tfr cells have been shown to broadly inhibit autoantibody responses, studies have indicated both positive and negative effects of Tfr cells in foreign antigen specific responses. We recently showed that Tfr cells set activation thresholds on the GC reaction during vaccination and therefore can promote somatic hypermutation and affinity maturation¹⁸. Our current study establishes the crucial role of Tfr cells in rejection using a Tfr-DTR mouse model that perturbs Tfr cells without affecting other Treg populations. We demonstrated that the absence of Tfr cells in kidney recipients leads to reduced renal graft survival, heightened pathological manifestations of ABMR-like disease (with less, if any, effects on TCMR-like disease) in grafts, and elevated serologic DSA levels. Although previous studies have shown that CXCR5⁺ CD8 T cells can influence DSA production⁴⁵, our data show that the regulatory effects of Tfr cells on B cell alloimmunity do not require CD8 T cells. The ability of Tfr cells to limit rejection was only found during the early stages of rejection, suggesting early suppression of Tfh and GC B cells is important to control ABMR-like disease. However, since the Tfr-DTR model may lose deletion potency over time as a consequence of host antibodies neutralizing DT, it is possible Tfr cells may have additional roles at other timepoints. These findings provide the first clear evidence of the negative regulatory role of Tfr in kidney transplantation, particularly in the context of ABMR. Moreover, these data suggest that promoting Tfr cells early after kidney transplantation may have the most robust and durable responses clinically.

Mechanistically, we found that Tfr cell suppression of rejection occurred through regulation of DSA-specific B cell responses both in lymph nodes and within kidney allografts. Since Tfh cells can promote pathogenic B cell responses both in lymph nodes and grafts²⁵, this suggests Tfr cells may limit Tfh-induced B cell responses wherever they occur. Tfr suppression of ABMR-like disease was achieved, in part, through the transcriptional reprogramming of GC B cells which included limiting production of cytokines such as IL-15. Inhibiting IL-15 antagonized the accelerated rejection in Tfr-DTR mice. Although IL-15 is a pleiotropic cytokine that has effects on many cell types involved in rejection including CD8 T cells and NK cells, it can also affect Tfh and B cell responses. Some studies have reported that IL-15 stimulates B cell proliferation and differentiation⁴⁶, and controls immature B-cell homing⁴⁷. Moreover, IL-15 can enhance Bcl6 expression and promote Tfh cell responses⁴⁸. Mechanistically dissecting the multifaceted roles of IL-15 in vivo is difficult due to broad and mechanistically complex sensing of this cytokine. However, our study suggest B cells can make IL-15 to promote Tfh cells, which in turn promote further GC B cell responses. It is important to note that our study cannot exclude the involvement of non-B cells in IL-15 mediated responses, nor can it fully differentiate between the effects of trans-presented versus non-trans-presented IL-15 in vivo. Although Tfr-mediated regulation of IL-15 in GC B cells may be only one of several factors in ABMR-like disease, the involvement of IL-15 in Tfh/GC B, CD8 T, and NK cells suggests synergy amongst multiple arms of the immune system. Moreover, although CD8 T cells were not required for the increased rejection in Tfr-deleted mice, it is possible that TCMR and ABMR-like diseases may be intertwined through the IL-15 pathway. Together, our data suggest that Tfr cells have potent roles in limiting ABMR-like disease indicating enhancing Tfr cells after transplantation may be a strategy to provide durable prevention of ABMR.

Methods

Animals

All animal research was conducted according to the guidelines of the Brigham and Women's Hospital Institutional Animal Care and Use

Committee and National Institute of Health. Balb/c (#000651), IL-15Rα KO (#003723) and B6129SF2/J (#101045), *Ighm*^{-/-} (μMT, #002288) mice were obtained from Jackson Laboratories. The *Foxp3*^{ires-GFP} and Tfr-DTR (*Foxp3*^{ires-CreYFP} *Cxcr5*^{ires-LoxP-STOP-LoxP-DTR}) mice on the C57BL/6 background were previously published¹⁸. Experimental and control mice were co-housed in a specific pathogen-free facility, under 12/12 h dark/light cycle, at 22 °C and 42% humidity. Males and females between 6 and 10 weeks of age were used in the study. Mice were fed 5053 PicoLab rodent diet 20 (LabDiet). Mice were humanely euthanized using CO₂ inhalation followed by cervical dislocation as confirmation.

Mouse kidney transplantation and treatment

The left kidney from the donor was transplanted along with its ureter into the abdominal cavity of the recipient mice^{2,25,27}. The donor kidney's artery and vein were connected to the recipient's abdominal aorta and vena cava, respectively, using 10-0 sutures in an "end-to-side" manner. To reconstruct the urinary tract, the graft's ureter was implanted into the recipient's bladder. The surgical procedures typically lasted for 2 h, including an approximately 25-minute anastomotic phase. The recipients were harvested on day 20 post-transplantation as indicated. For the life-sustaining surgeries, the ureters of the remaining native kidneys were ligated on postoperative days 2–4 to limit function. This procedure renders the transplanted kidney the only kidney supporting the life of the recipient, and mechanistically maintains the rejection process similar to non-survival surgeries (Supplementary Fig. 12). On day 2 after the transplantation procedure, a dose of 250 μg of CTLA4Ig (Abatacept, Bristol-Myers Squibb) was administered via intraperitoneal injection. Deletion experiments involved intraperitoneal administration of 0.5 μg of diphtheria toxin in PBS at the specified time points. To block IL-15 signaling, 200 μg of anti-mouse IL-15 (Clone: AIO.3, Bioxcell, #BE0315) was administered intravenously five times (day 3, 6, 9, 12, 15) after kidney transplantation. For CD8 depletion, 200 μg of rat anti-mouse CD8a (clone 2.43, Bioxcell, #BE0061) was administered intraperitoneally beginning on day 0 and continued every 4 days until 20 days post-transplantation.

Donor-specific antibody (DSA) measurements

For the determination of DSA, we used a flow cytometric crossmatch (FCXM) assay. Fresh splenocytes (5 × 10⁵) from donor wildtype Balb/c mice were incubated with recipients' serum samples at 1:50 dilution for IgG, or undiluted supernatant from single-cell cultures for 30 minutes, allowing DSA to bind to specific antigens on the surface of the donor cells. Next, the splenocytes were stained with anti-CD19 (6D5, Biolegend) in the presence of Fc-block (Biolegend) followed by an additional stain using FITC-labeled anti-IgG or anti-IgM. For assays involving single alloantigens, MHC beads (K^b, K^d, L^d, I-A^d, I-E^d) were incubated with serum at a dilution of 1:50 or serial dilution at 4 °C for 1 h^{49,50}. Bound antibodies were detected using FITC-labeled anti-IgG. The signal of bound IgG on CD19⁺ splenocytes was measured and expressed as mean fluorescence intensity (MFI).

Flow cytometry

Antibodies were purchased from BioLegend unless otherwise stated. Mouse antibodies (with their clone numbers, 1:200 dilution unless otherwise specified) against the following proteins were used: anti-CD4 (GK1.5), anti-CD19 (1D3), anti-ICOS (15F9), anti-CXCR5 (L138D7), anti-PD-1 (RMP1-30), anti-FoxP3 (eBiosciences, FJK-16s), anti-CD45 (30-F11), anti-CD38 (90/CD38), anti-GL7 (GL-7), anti-FAS (BD Biosciences, JO2), anti-IgG1 (BD Biosciences, A85-1), anti-IgG (SouthernBiotech), anti-Ki67 (16A8), anti-IL-15Rα (6B4C88), anti-CD44 (IM7), anti-CD62L (MEL-14), anti-CD69 (H1.2F3), anti-Ly6C (HK1.4), anti-TIGIT (1G9), anti-FR4 (eBiosciences, eBio12A5), anti-CD73 (TY/IL8), anti-CD8 (53-6.7) and LIVE/DEAD Fixable Blue Dead Cell Stain Kit (1:1000, Invitrogen) was used to label cells live/dead. The catalog numbers are listed in the Reporting Summary. Single-cell suspensions of draining lymph nodes,

spleen, and grafts were prepared. Ficoll-paque (Cytiva) was utilized following the published protocol to separate graft-infiltrating lymphocytes. Surface marker staining was done at 4 °C for 30 min. The Foxp3 Fix/Perm buffer set was used as per the manufacturer's instructions (eBioscience) for intracellular staining. For intracellular cytokine staining, cells were stimulated with Cell Activation Cocktail (BioLegend) for 4 h, then permeabilized and stained with corresponding antibodies. Fluorescence signals were detected using a Cytex Aurora flow cytometer and analyzed with FlowJo software.

Bulk RNA sequencing

We conducted RNA-seq using an Illumina NextSeq sequencer with 50-basepair reads and analyzed the data using CLC Genomics Workbench v.8.0.1 by Qiagen. Differently expressed genes (DEGs) were filtered by at least 2-fold change and p -value < 0.05. We analyzed the Kyoto Encyclopedia of Genes and Genomes (KEGG) on the DAVID website (<https://david.ncifcrf.gov/>) with a p -value cut-off of 0.05.

Single cell RNAseq and analysis

Draining lymph nodes from allogeneic kidney transplant recipients who did or did not receive CTLA4Ig treatment were harvested 20 days post-transplant. Single cell suspensions were stained with fluorochrome-labeled cell surface antibodies and distinct barcoded antibodies (Cell-Hashing antibody, TotalSeq-C, Biolegend)⁵¹. Live CD4⁺CD19⁺CXCR5⁺Foxp3⁺ Tfr and CD4⁺CD19⁺CXCR5⁺Foxp3⁺ naïve Treg cells were sorted from each mouse group, pooled together, and resuspended in PBS 0.4% BSA at a concentration of 2000 cells/μl. Samples were subsequently loaded onto a single lane (Chromium chip K, 10X Genomics) followed by encapsulation (Single Cell 5'kit V2, 10X Genomics) at the Brigham and Women's Hospital Single Cell Genomics Core. cDNA and library generation were performed according to the manufacturer's protocol. The 5' mRNA library was sequenced to an average of 50,000 reads per cell, whereas the V(D)J library and HTO (Cell Hashing antibodies) library were both sequenced to an average of 5000 reads per cell, all using Illumina Novaseq. Reads were processed with Cell Ranger, and quantification was performed using the STAR aligner against the mm10 transcriptome. CellRanger output data were loaded into the R programming environment and analyzed with the Seurat package. Sample demultiplexing and doublet exclusion were performed with the HTODemux function, and only singlets were selected for further analysis. Additional quality-control filtering was performed, imposing as thresholds unique UMI counts ≥ 2000, UMI counts < 15000, gene counts ≥ 1000, log-transformed genes per UMI > 0.8 and mitochondrial RNA content < 4%. Count data were subjected to normalization and variance stabilization using the SCTransform function (v.2), based on the 3000 most variable genes and by concomitantly regressing cell-cycle phase, mitochondrial, and ribosomal mapping percentages. Additional filtering based on identity was applied after a comparison of each cell with the Immunologic Genome Project dataset (using the SingleR pipeline), to exclude contaminating cells (e.g. CD8⁺ T, and NKT cells)⁵². Uniform manifold approximation and projection (UMAP) was used for dimensionality reduction according to the standard Seurat pipeline, but TCR-related genes were excluded from the list of variable features to avoid clustering based on clonotype. Differential gene expression was computed with the FindAllMarkers command (logFC threshold = 0.1, min.pct = 0.1) and module scores were calculated with the AddModuleScore function, using as input a previously generated gene set comprising upregulated genes in Tfr compared to Treg cells in our bulk RNAseq dataset. Differential abundance analysis across clusters between untreated and CTLA4Ig mouse samples was conducted with miloR⁵³. TCR clonotype analysis was performed with the scRepertoire package⁵⁴. Pseudotime trajectory analysis was carried out with Monocle3⁵⁵.

In Vitro functional assays

Tfh, Tfr, and B cells were isolated from spleens of FoxP3 reporter, IL15Rα KO or B6129SF2/J mice post-20 days allogeneic kidney transplantation. In vitro assays involved co-culturing 5×10^4 B cells with 3×10^4 Tfh or Tfr cells in 96-well U bottom plates, stimulated with anti-CD3 (2 μg/mL, Bioxcell, 2C11) and anti-IgM (5 μg/mL, Jackson ImmunoResearch), and maintained in a complete medium (RPMI-1640 supplemented with 10% FBS and 1% penicillin-streptomycin) at 37 °C and 5% CO₂ for 4 days. Cultures were maintained in complete medium for 4 days. To block IL-15 signaling, 100 ng/ml of anti-mouse IL-15 (Clone: AIO.3, Bioxcell) was supplemented to each well. Subsequent to the culture period, cells and supernatants were harvested for flow cytometry and ELISA.

Single B cell cultures

Single GC B cells (CD45⁺B220⁺CD4⁺GL7⁺CD38^{lo/-}) from lymph nodes and kidney grafts were isolated and individually sorted into 96-well plates containing 1×10^3 NB21.2D9 feeder cells (provided by Garnett Kelsoe, Duke University, Durham, North Carolina, USA). The cells were cultured for 6 days, and IgG-positive clones were identified via ELISA. Clones positive for IgG were subsequently tested for DSA reactivity as above.

ELISA

To determine serum or cell culture supernatant levels of IL-15, IL-2 and IFN-γ, mouse ELISA Kits (ThermoFisher) were used according to the instructions of the manufacturer. At 450 nm, the OD values of each sample were measured to express the concentration of cytokines.

Histopathological staining

Graft samples were harvested and either immediately submerged in 10% formalin for embedding in paraffin or preserved in Tissue-Tek OCT Compound. Hematoxylin and eosin (HE), immunohistochemistry (IHC) and immunofluorescence (IF) staining were carried out⁵⁶. The antibodies employed in the experiments included anti-CD3 (D4V8L, 1:100), anti-CD4 (D7D2Z, 1:100), anti-CD8 (D4W2Z, 1:500), anti-CD68 (E307V, 1:200), from Cell Signaling Technology, anti-B220 (RA3-6B2, 1:200), anti-GL7 (GL7, 1:100), anti-IgD (11-26 c.2a, 1:500) from Biolegend, anti-MHCII-I-A/I-E(M5/114.15.2) from eBioscience and C4d (16D2, 1:100) from Novus Biologicals. The catalog numbers are listed in the Reporting Summary. Microscopic images were captured using a ZEISS Axiolab 5 microscope. Pathological manifestations were evaluated based on Banff 2018 classification⁵⁷ with i (interstitial inflammation), t (tubulitis), g (glomerulitis), ptc (peritubular capillaritis) and v (vasculitis) components.

Autoantibody detection

For autoantibody detection, we used the Hep-2 antibody detection kit according to the manufacturer's instructions. The serum samples were applied to Hep-2-coated slides and incubated to allow binding of autoantibodies to antigens. Post-wash, fluorophore-conjugated secondary antibodies were added, binding to the primary antibodies. After a final wash, slides were examined under a fluorescence microscope, capturing images for analysis.

Statistics

Student's unpaired t-test or Mann-Whitney test were used as indicated utilizing GraphPad Prism, version 9 (GraphPad Software). Multiple comparisons were conducted using one-way ANOVA followed by Tukey's test. Graft survival was compared using Kaplan-Meier survival analysis and a log-rank test. We considered significance at a P value below 0.05. The graphs depict values that represent the standard error of the mean (SEM), NS: not significant; * P < 0.05; ** P < 0.01, *** P < 0.001.

Reporting summary

Further information on research design is available in the Nature Portfolio Reporting Summary linked to this article.

Data availability

The sequencing data generated in this study have been deposited in the GEO database under [GSE286975](https://www.ncbi.nlm.nih.gov/geo/query/acc.cgi?acc=GSE286975). All data are included in the Supplementary Information or available from the authors, as are unique reagents used in this Article. The raw numbers for charts and graphs are available in the Source Data file whenever possible. Source data are provided with this paper.

References

1. Vanholder, R. et al. Organ donation and transplantation: a multi-stakeholder call to action. *Nat. Rev. Nephrol.* **17**, 554–568 (2021).
2. Zhang, H. et al. Transcriptionally Distinct B Cells Infiltrate Allografts After Kidney Transplantation. *Transplantation* **107**, e47–e57 (2023).
3. Gassen, R. B. et al. T cell depletion increases humoral response by favoring T follicular helper cells expansion. *Am. J. Transpl.* **22**, 1766–1778 (2022).
4. Wojciechowski, D. & Wiseman, A. Long-Term Immunosuppression Management: Opportunities and Uncertainties. *Clin. J. Am. Soc. Nephrol.* **16**, 1264–1271 (2021).
5. Mohiuddin, M. M. et al. Graft dysfunction in compassionate use of genetically engineered pig-to-human cardiac xenotransplantation: a case report. *Lancet* **402**, 397–410 (2023).
6. Loupy, A. et al. Immune response after pig-to-human kidney xenotransplantation: a multimodal phenotyping study. *Lancet* **402**, 1158–1169 (2023).
7. Louis, K., Macedo, C., Lefaucheur, C. & Metes, D. Adaptive immune cell responses as therapeutic targets in antibody-mediated organ rejection. *Trends Mol. Med* **28**, 237–250 (2022).
8. Chong, A. S., Rothstein, D. M., Safa, K. & Riella, L. V. Outstanding questions in transplantation: B cells, alloantibodies, and humoral rejection. *Am. J. Transpl.* **19**, 2155–2163 (2019).
9. Crotty, S. T Follicular Helper Cell Biology: A Decade of Discovery and Diseases. *Immunity* **50**, 1132–1148 (2019).
10. Tas, J. M. et al. Visualizing antibody affinity maturation in germinal centers. *Science* **351**, 1048–1054 (2016).
11. Sage, P. T., Paterson, A. M., Lovitch, S. B. & Sharpe, A. H. The coinhibitory receptor CTLA-4 controls B cell responses by modulating T follicular helper, T follicular regulatory, and T regulatory cells. *Immunity* **41**, 1026–1039 (2014).
12. Sage, P. T., Francisco, L. M., Carman, C. V. & Sharpe, A. H. The receptor PD-1 controls follicular regulatory T cells in the lymph nodes and blood. *Nat. Immunol.* **14**, 152–161 (2013).
13. Sage, P. T. & Sharpe, A. H. T follicular regulatory cells. *Immunol. Rev.* **271**, 246–259 (2016).
14. Wing, J. B., Lim, E. L. & Sakaguchi, S. Control of foreign Ag-specific Ab responses by Treg and Tfr. *Immunol. Rev.* **296**, 104–119 (2020).
15. Fonseca, V. R., Ribeiro, F. & Graca, L. T follicular regulatory (Tfr) cells: Dissecting the complexity of Tfr-cell compartments. *Immunol. Rev.* **288**, 112–127 (2019).
16. Hou, S. et al. FoxP3 and Ezh2 regulate Tfr cell suppressive function and transcriptional program. *J. Exp. Med* **216**, 605–620 (2019).
17. Wing, J. B. et al. A distinct subpopulation of CD25(–) T-follicular regulatory cells localizes in the germinal centers. *Proc. Natl. Acad. Sci. USA* **114**, E6400–E6409 (2017).
18. Clement, R. L. et al. Follicular regulatory T cells control humoral and allergic immunity by restraining early B cell responses. *Nat. Immunol.* **20**, 1360–1371 (2019).
19. Cavazzoni, C. B. et al. Follicular T cells optimize the germinal center response to SARS-CoV-2 protein vaccination in mice. *Cell Rep.* **38**, 110399 (2022).
20. Sage, P. T. et al. Suppression by T(FR) cells leads to durable and selective inhibition of B cell effector function. *Nat. Immunol.* **17**, 1436–1446 (2016).
21. Jandl, C. et al. IL-21 restricts T follicular regulatory T cell proliferation through Bcl-6 mediated inhibition of responsiveness to IL-2. *Nat. Commun.* **8**, 14647 (2017).
22. Sage, P. T. Preventing Antibody-mediated Rejection During Transplantation: The Potential of Tfr Cells. *Transplantation* **102**, 1597–1598 (2018).
23. Mohammed, M. T. & Sage, P. T. Follicular T-cell regulation of alloantibody formation. *Curr. Opin. Organ Transpl.* **25**, 22–26 (2020).
24. Zhang, H. & Sage, P. T. Role of T follicular helper and T follicular regulatory cells in antibody-mediated rejection: new therapeutic targets? *Curr. Opin. Organ Transpl.* **27**, 371–375 (2022).
25. Zhang, H. et al. IL-21-producing effector Tfh cells promote B cell alloimmunity in lymph nodes and kidney allografts. *JCI Insight* **8**, e169793 (2023).
26. Niu, Q. et al. Immunosuppression Has Long-Lasting Effects on Circulating Follicular Regulatory T Cells in Kidney Transplant Recipients. *Front Immunol.* **11**, 1972 (2020).
27. Mohammed, M. T. et al. Follicular T cells mediate donor-specific antibody and rejection after solid organ transplantation. *Am. J. Transpl.* **21**, 1893–1901 (2021).
28. Charpentier, B. et al. Long-term exposure to belatacept in recipients of extended criteria donor kidneys. *Am. J. Transpl.* **13**, 2884–2891 (2013).
29. Grinyo, J. M. et al. Safety and Efficacy Outcomes 3 Years After Switching to Belatacept From a Calcineurin Inhibitor in Kidney Transplant Recipients: Results From a Phase 2 Randomized Trial. *Am. J. Kidney Dis.* **69**, 587–594 (2017).
30. Schulte, K. et al. Late conversion from tacrolimus to a belatacept-based immuno-suppression regime in kidney transplant recipients improves renal function, acid-base derangement and mineral-bone metabolism. *J. Nephrol.* **30**, 607–615 (2017).
31. Fu, W. et al. Deficiency in T follicular regulatory cells promotes autoimmunity. *J. Exp. Med.* **215**, 815–825 (2018).
32. Asano, Y. et al. Innate-like self-reactive B cells infiltrate human renal allografts during transplant rejection. *Nat. Commun.* **12**, 4372 (2021).
33. Podesta, M. A. et al. Stepwise differentiation of follicular helper T cells reveals distinct developmental and functional states. *Nat. Commun.* **14**, 7712 (2023).
34. Komlosi, Z. I. et al. Human CD40 ligand-expressing type 3 innate lymphoid cells induce IL-10-producing immature transitional regulatory B cells. *J. Allergy Clin. Immunol.* **142**, 178–194 e111 (2018).
35. Rafei, M. et al. A granulocyte-macrophage colony-stimulating factor and interleukin-15 fusokine induces a regulatory B cell population with immune suppressive properties. *Nat. Med* **15**, 1038–1045 (2009).
36. Patidar, M., Yadav, N. & Dalai, S. K. Interleukin 15: A key cytokine for immunotherapy. *Cytokine Growth Factor Rev.* **31**, 49–59 (2016).
37. Schinstock, C., Tambur, A. & Stegall, M. Current Approaches to Desensitization in Solid Organ Transplantation. *Front. Immunol.* **12**, 686271 (2021).
38. Shim, Y. J. et al. Early T cell infiltration is modulated by programmed cell death-1 protein and its ligand (PD-1/PD-L1) interactions in murine kidney transplants. *Kidney Int* **98**, 897–905 (2020).
39. Sun, H. et al. TIGIT regulates apoptosis of risky memory T cell subsets implicated in belatacept-resistant rejection. *Am. J. Transpl.* **21**, 3256–3267 (2021).
40. Wyatt, C. M. & Arons, R. R. The burden of acute renal failure in nonrenal solid organ transplantation. *Transplantation* **78**, 1351–1355 (2004).

41. Bluestone, J. A., St Clair, E. W. & Turka, L. A. CTLA4Ig: bridging the basic immunology with clinical application. *Immunity* **24**, 233–238 (2006).
42. Vincenti, F. et al. Belatacept and Long-Term Outcomes in Kidney Transplantation. *N. Engl. J. Med.* **374**, 333–343 (2016).
43. Sakaguchi, S., Yamaguchi, T., Nomura, T. & Ono, M. Regulatory T cells and immune tolerance. *Cell* **133**, 775–787 (2008).
44. Hartigan, C. R., Tong, K. P., Liu, D., Laurie, S. J. & Ford, M. L. TIGIT agonism alleviates costimulation blockade-resistant rejection in a regulatory T cell-dependent manner. *Am. J. Transpl.* **23**, 180–189 (2023).
45. Zimmerer, J. M. et al. Antibody-suppressor CXCR5(+) CD8(+) T cellular therapy ameliorates antibody-mediated rejection following kidney transplant in CCR5 KO mice. *Am. J. Transpl.* **22**, 1550–1563 (2022).
46. Armitage, R. J., Macduff, B. M., Eisenman, J., Paxton, R. & Grabstein, K. H. IL-15 has stimulatory activity for the induction of B cell proliferation and differentiation. *J. Immunol.* **154**, 483–490 (1995).
47. Hart, G., Avin-Wittenberg, T. & Shachar, I. IL-15 regulates immature B-cell homing in an Ly49D-, IL-12, and IL-18 dependent manner. *Blood* **111**, 50–59 (2008).
48. Cooley, I. D., Read, K. A. & Oestreich, K. J. Trans-presentation of IL-15 modulates STAT5 activation and Bcl-6 expression in TH1 cells. *Sci. Rep.* **5**, 15722 (2015).
49. Yang, J. et al. Tracing Donor-MHC Class II Reactive B cells in Mouse Cardiac Transplantation: Delayed CTLA4-Ig Treatment Prevents Memory Alloreactive B-Cell Generation. *Transplantation* **100**, 1683–1691 (2016).
50. Young, J. S., McIntosh, C., Alegre, M. L. & Chong, A. S. Evolving Approaches in the Identification of Allograft-Reactive T and B Cells in Mice and Humans. *Transplantation* **101**, 2671–2681 (2017).
51. Stoeckius, M. et al. Cell Hashing with barcoded antibodies enables multiplexing and doublet detection for single cell genomics. *Genome Biol.* **19**, 224 (2018).
52. Aran, D. et al. Reference-based analysis of lung single-cell sequencing reveals a transitional profibrotic macrophage. *Nat. Immunol.* **20**, 163–172 (2019).
53. Dann, E., Henderson, N. C., Teichmann, S. A., Morgan, M. D. & Marioni, J. C. Differential abundance testing on single-cell data using k-nearest neighbor graphs. *Nat. Biotechnol.* **40**, 245–253 (2022).
54. Borcherting, N., Bormann, N. L. & Kraus, G. scRepertoire: An R-based toolkit for single-cell immune receptor analysis. *F1000Res* **9**, 47 (2020).
55. Trapnell, C. et al. The dynamics and regulators of cell fate decisions are revealed by pseudotemporal ordering of single cells. *Nat. Biotechnol.* **32**, 381–386 (2014).
56. Zhang, H. et al. Combined Immunotherapy With Belatacept and BTLA Overexpression Attenuates Acute Rejection Following Kidney Transplantation. *Front Immunol.* **12**, 618737 (2021).
57. Roufosse, C. et al. A 2018 Reference Guide to the Banff Classification of Renal Allograft Pathology. *Transplantation* **102**, 1795–1814 (2018).

Acknowledgements

We would like to thank Dr. Marcus Clark for help with autoreactivity assays and Dr. Garnett Kelsoe for reagents. This work was funded through grants from the National Institute of Health, P01AI056299, P01AI175397, R01AI153124 to P.T.S. and R35HL166640 to R.A. P.L.R. received a scholarship from The São Paulo Research Foundation (2022/07035-3). Portions of figures were created with BioRender.com.

Author contributions

H.Z. designed and performed experiments, acquired and analyzed data, and wrote the manuscript. M.A.P. and C.B.C. performed experiments and analyzed data. Y.W., J.L., X.L., P.L.R., P.C., M.G., S.R., and I.S. performed experiments. D.G., B.R.B., R.A., A.W. and A.S.C. provided key technical help. P.T.S. designed experiments, analyzed data, secured funding, and wrote the manuscript. All authors edited the manuscript.

Competing interests

The authors declare no competing interests.

Additional information

Supplementary information The online version contains supplementary material available at <https://doi.org/10.1038/s41467-025-57468-4>.

Correspondence and requests for materials should be addressed to Peter T. Sage.

Peer review information *Nature Communications* thanks Jean Kwun and the other anonymous reviewer(s) for their contribution to the peer review of this work. A peer review file is available.

Reprints and permissions information is available at <http://www.nature.com/reprints>

Publisher's note Springer Nature remains neutral with regard to jurisdictional claims in published maps and institutional affiliations.

Open Access This article is licensed under a Creative Commons Attribution-NonCommercial-NoDerivatives 4.0 International License, which permits any non-commercial use, sharing, distribution and reproduction in any medium or format, as long as you give appropriate credit to the original author(s) and the source, provide a link to the Creative Commons licence, and indicate if you modified the licensed material. You do not have permission under this licence to share adapted material derived from this article or parts of it. The images or other third party material in this article are included in the article's Creative Commons licence, unless indicated otherwise in a credit line to the material. If material is not included in the article's Creative Commons licence and your intended use is not permitted by statutory regulation or exceeds the permitted use, you will need to obtain permission directly from the copyright holder. To view a copy of this licence, visit <http://creativecommons.org/licenses/by-nc-nd/4.0/>.

© The Author(s) 2025